Mesooptics and the track-detector technique

L. M. Soroko

Joint Institute for Nuclear Research, Dubna

Fiz. Elem. Chastits At. Yadra **20**, 155–197 (January–February 1989)

The current techniques for solving the problem of the depth of focus in track chambers, in particular, in nuclear photoemulsion are reviewed. In the first half of the review we discuss the main features of the techniques for solving this problem by means of the wave-field hologram, the intensity hologram, and the optical objective with an annular aperture. The second half of the review is devoted to mesooptics and mesooptical imaging systems. The mesooptical Fourier-transform microscope for nuclear photoemulsion, mesooptical microscopes for vertical particle tracks, and the mesooptical condenser based on the tomography principle are described. The results of some experiments carried out using mock-up systems of some of these devices are given. The review concludes with a brief comparison of the advantages and disadvantages of these methods. It is pointed out that mesooptics is suitable for reading out information from holograms of particle tracks, in traditional systems for scanning and measuring photographs produced in track detectors with a magnetic field, and in photographic systems in place of the traditional photographic objective.

INTRODUCTION

The track detectors used in high-energy physics have long had the problem of obtaining a high spatial resolution in a volume whose dimensions are much greater than the depth of focus of classical imaging optics. This problem became more acute when the properties of elementary particles with very short lifetimes, 10^{-13}–10^{-15} sec, began to be studied. The performance of an experimental setup came to be determined by its absolute, rather than relative, spatial resolution. Progress was achieved after the operation of observing a nuclear interaction vertex was separated from the operation of measuring the kinematic parameters of the secondary particles. The technique of hybrid experiments using a vertex detector and an external secondary-particle spectrometer was developed. Miniature rapid-cycling bubble or streamer chambers, semiconductor detectors, or nuclear photoemulsion were used as the vertex detector.

Meanwhile, the problem of the depth of focus remained unsolved. The observation of short-lived elementary particles in bubble chambers required a spatial resolution of about 10 μm. Classical imaging optics allowed such a resolution to be obtained only for a depth of about 1 mm. This was 100 times smaller than the depth of focus of a miniature track chamber. The spatial resolution in nuclear photoemulsion is 0.5 μm, which corresponds to a depth of focus of 3 μm, or 70 times smaller than 200 μm, the total thickness of the nuclear-photoemulsion layer. Since the density of useful events in nuclear photoemulsion is small, while the background of fog from silver grains is very large, here it is impossible to use optics with a small spatial resolution for the complete scanning of a large volume of nuclear photoemulsion. A large amount of time would be spent on the laborious search for useful events.

Solutions to the depth-of-focus problem in track- and emulsion-chamber techniques have been sought in various ways. These are: 1) wave-field holograms with the track-chamber volume exposed to a coherent beam of laser light; 2) intensity holograms with partially coherent illumination; 3) optical objectives with an annular aperture; 4) mesooptical imaging systems.

Here we shall review the main features of these four approaches to solving the depth-of-focus problem in track detectors, and we shall compare their advantages and disadvantages. A considerable part of the review is devoted to mesooptics. This is because mesooptics provides a solution to the problem of the depth of focus in nuclear photoemulsion and makes it possible to select useful particle tracks and nuclear interactions much more quickly than when the traditional optical microscope is used. In this review we describe the mesooptical Fourier-transform microscope for nuclear photoemulsion, mesooptical microscopes for vertical particle tracks, and the mesooptical condenser with operating principle borrowed from reconstructive tomography. We show how mesooptics can be used for reading out information from holograms, and also in traditional systems for scanning and measuring photographs obtained in track chambers with a magnetic field.

1. THE WAVE-FIELD HOLOGRAM WITH COHERENT ILLUMINATION

The stage of obtaining the holograms

It was first shown in the experiments of Refs. 1 and 2 that holography can be used to detect particle tracks with bubbles of diameter 60 μm. Two goals were achieved by this: the depth of focus was increased, and the charging capacity of the bubble chamber by the beam particles was raised. At first it was thought that the Leith hologram with separated reference and object beams of coherent light was the most effective.[3,4] However, it was later found that pointlike elements of a particle track could be detected using two[5] or one Gabor holograms.[6] The current technique of illuminating the track chamber by a collimated beam of light appears to be the simplest[7] (Fig. 1). A collimated beam of laser light illuminates the volume of a track chamber having two optical windows and falls directly on the photographic film. In order to detect a track element of diameter d on the hologram, the transverse dimension of the hologram $2a$ must be chosen in conformity with the condition

$$d \geq 1.22\lambda R/2a, \tag{1}$$

 0090-4759/89/010067-19$04.40

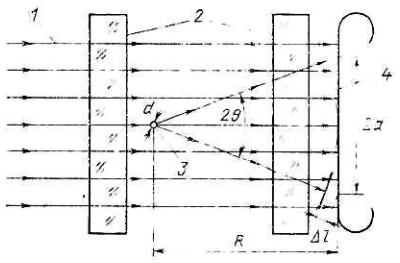

FIG. 1. Basic scheme for obtaining a Gabor hologram: 1—collimated beam of laser light; 2—optical windows of the track chamber; 3—bubble; 4—photographic film on which the hologram is made.

where λ is the wavelength of the light and R is the distance from the track element to the hologram. Condition (1) must be satisfied in order for most of the light diffracted on the most distant element of the particle track to fall on the hologram. For the most distant element of the particle track the difference between the path of a light ray scattered at an angle $\theta \sim 0.6\lambda/d$ and the path of a light ray which has not undergone diffraction is

$$\Delta l \approx \frac{R}{12}\left(\frac{\lambda}{d}\right)^2. \qquad (2)$$

The coherence length of the light, L, must not be smaller than Δl. We see from (2) that the larger the element of the particle track, the smaller the required coherence length L. If $d = 10\,\mu$m and $\lambda = 0.5\,\mu$m, for $L = 2$ mm the Gabor hologram gives a depth of focus $\Delta z \approx 10$ m (!). However, the dimension of the hologram must be $2a \cong 50$ cm.

Holograms of focused images are used to decrease the size of the photographic film on which the hologram is made.[8–10] In Fig. 2 we give a schematic diagram for obtaining a focused-image hologram[11] using the Leith scheme. The technique of focused-image holography makes it possible to estimate the position of a track element of diameter 10 μm with an error of 2.5 μm in the plane of the hologram and 30 μm in the depth.[11]

Systematic studies of the conditions for obtaining holograms in a rapid-cycling heavy-liquid bubble chamber[12,13] have confirmed the fact that holography can be used to reliably detect bubbles of diameter 6 μm in the liquid when the distance from the center of the chamber to the hologram is 8 cm. The reconstructed image of the track of a primary

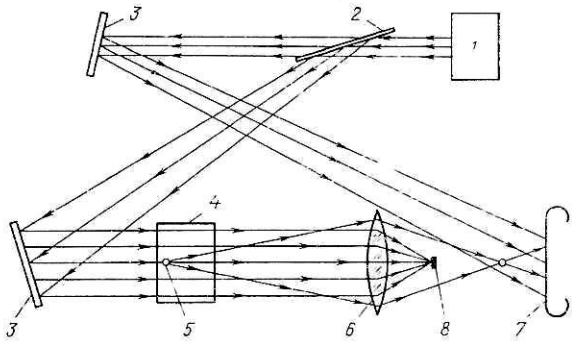

FIG. 2. Basic scheme for obtaining a two-ray Leith focused-image hologram of scale $M = l_1/l_2$: 1—laser; 2—beam splitter; 3—plane mirrors; 4—chamber volume; 5—bubble; 6—collecting lens; 7—photographic plate for obtaining the hologram; 8—direct light-beam filter.

charged particle with minimum ionization contains 100–120 bubbles in a track length of 1 cm. The cycling rate reaches 10 Hz. It was simultaneously discovered that turbulence in the liquid during the growth and recompression of the bubbles leads to distortions, which could partially be eliminated by going to the "hot" chamber regime. A resolution of 10 μm was also obtained in a small Wilson chamber of dimensions $7.5 \times 7.5 \times 7$ cm using a Gabor hologram.[14] The cycling period of the chamber was 20 sec.

It was shown in Ref. 15 that, when the holography technique is used to obtain ever higher spatial resolutions, limitations arise owing to aberrations in the optical windows of the bubble chambers during the stage at which the hologram is made and also to similar effects during the reconstruction stage.[16]

Studies on the use of holography in streamer chambers have developed dramatically. At first, streamers were photographed by detecting the streamer "shadowgram" in the transmitted light from a laser.[17] This made it possible to eliminate light amplification.[18] The authors of Ref. 19 obtained the first Leith holograms in a helium discharge chamber at a pressure of 1 atm. The angle between the reference and object light beams was 30°. The reconstructed image of a particle track obtained by the double-exposure method contained 3–4 elements over a length 1 cm, an element of the particle track being 0.5–2 mm in length and 0.5–2 mm in diameter. In subsequent studies a "shadowgram" was detected with a single light beam.[20] Two thousand "shadowgrams" of tracks of 1-GeV protons and nuclear interactions were obtained. The streamer dimensions were 0.38 mm in the direction perpendicular to the electric field and 2.5 mm along the field. This was an important step forward from the method of direct photography of streamers via their luminosity, for which the streamer dimensions were 1.5 and 6.2 mm, respectively. The reason for this difference is that in the method where the self-luminous streamer is photographed directly the observer sees the "photosphere" of the streamer, whereas with external illumination only the core of the streamer with maximum optical nonuniformity is seen.[21] The spatial localization of the streamer is improved by a factor of 4:1 (Ref. 24). In Refs. 21–23 it was shown that the difference between the indices of refraction of light in the streamer, n, and in the surrounding gas, n_0, is $\Delta n = n_0 - n \approx 0.5 \times 10^{-4}$ when the gas is at atmospheric pressure and the electric field is 40 kV/cm, when the diameter of the streamer neck is 0.5 mm. The structure of the streamer "shadowgram" depends on the time interval Δt between the beginning of the discharge and the detection time. For $\Delta t > 400$–500 nsec a shock wave leaves the streamer.[25]

The first holographic detection of electron tracks in a hydrogen streamer chamber was done in Ref. 26. The diameter of the working volume of the chamber was 25 cm and the height was 7 cm. The self-shunting regime[29,30] was used without the introduction of localizing impurities.[27,28,31]

In an operating streamer chamber with a magnetic field accessible only from one direction it was impossible to obtain a hologram[26] by a scheme like the Gabor scheme with direct illumination of the working volume of the chamber or by the method of focused-image holograms. Therefore, a stereoscopic method was developed using a spherical mirror and double passage of the light through the chamber volume.[32] A cylindrical lens was introduced in order to com-

pensate for the astigmatism in the illumination system.[33] The required depth of focus of the photodetector was twice the actual depth of the working volume of the chamber. Since the transverse dimensions of the streamers were 0.15 mm (Ref. 34), there was no serious problem with the depth of focus for the depth of the working volume of the chamber equal to 150 mm. As a result, the application of holography in streamer chambers has been inadequate. The results of Refs. 35 and 36 also confirm this.

In a helium–neon chamber at a pressure of 24 atm (Ref. 35) a spatial resolution of 50 μm was obtained in streamer photography using luminosity enhancement. In a helium chamber at a pressure of 8 atm (Ref. 36) the spatial resolution was 20–30 μm at a chamber depth of 23 mm. The working volume of the chamber was illuminated by a converging light beam, and the streamers were photographed using the dark-field scheme. The streamer diameter was 55 μm. This scheme is very efficient, since the required power of the light source is 5 times smaller than in holography. However, if the streamer diameter is decreased to 15 μm and the depth of the streamer chamber is 200 mm, then physicists are faced with the same problem of the depth of focus as in miniature bubble chambers. Below we shall consider alternative solutions to the depth-of-focus problem which are unrelated to detection via a wave-field hologram with coherent illumination.

The reconstruction stage

A scheme for observing the real image of particle tracks detected in a Gabor hologram (see Fig. 1) is shown in Fig. 3. In order to scan the entire volume of the track chamber, the distance between the hologram and the microscope objective is systematically varied, and the two-dimensional images thus obtained are transmitted to a video display. The scanning system HOLMES (Refs. 37 and 38) uses three objectives with different focal lengths and three television cameras, one of which has anamorphic optics. The quality of the reconstructed image was improved by means of a spatial filter[38] and a second transfer lens (Fig. 4). The errors in determining the coordinates of a particle-track element were $\Delta x = \Delta y = 2\,\mu$m and $\Delta z = 150\,\mu$m. The accuracy of the other television cameras was worse. The setup of Ref. 38 was used to scan 8000 holograms obtained in the small chamber HOBC with dimensions $5\times6\times11$ cm. A scanning system was developed for the same chamber.[39] The authors of Ref.

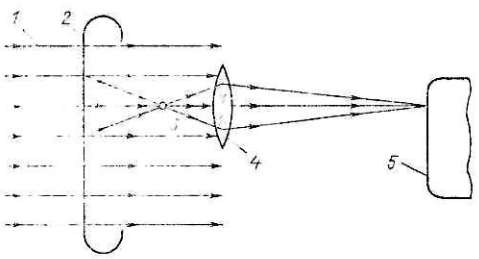

FIG. 3. Scheme for image reconstruction for a Gabor hologram: 1—collimated beam of laser light; 2—hologram; 3—real image of the bubble; 4—microscope objective; 5—observation screen.

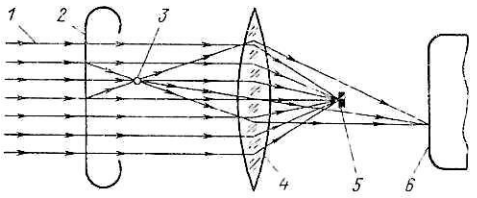

FIG. 4. Image-reconstruction scheme with spatial filtering: 1—collimated beam of laser light; 2—hologram; 3—real image of a bubble; 4—transfer lens; 5—spatial-frequency filter; 6—photodetector screen.

40 have analyzed the geometrical transformations of the reconstructed images which must be carried out in order that an operator can easily find a small-angle ($<4°$) kink in a particle track. Methods were studied for carrying out these transformations optically by transferring the original image from one plane to another using an inclined lens and an intermediate screen.

A three-dimensional semiautomatic scanning–measuring device for Gabor holograms[41] has been designed for a track chamber of dimensions $130\times50\times70$ mm. As in Ref. 38, the device contains an anamorphic objective and a spatial image-filtering system. The errors in measuring the position of the center of a bubble are $\Delta x = \Delta y = 5\,\mu$m and $\Delta z = 70\,\mu$m. The device operates rapidly, producing two holograms per hour. In Ref. 42, which is devoted to the analysis of experimental errors in an optical–television scheme for scanning Gabor holograms, it was shown that the errors for bubbles of diameter 5 μm were $\Delta x = \Delta y = 2.5\,\mu$m and $\Delta z = 20\,\mu$m.

Aberrations arising during image reconstruction for focused-image holograms were studied in Ref. 16. Here a high spatial resolution is obtained for small holograms. This leads to more stringent constraints on the degree of shrinkage of the photoemulsion layer, on the displacement of the hologram from the ideal location, and on the degree to which the reconstructive light wave deviates from a plane wave.

A measurement system[43] has been designed for measuring focused-image holograms in a system with an off-axis reference beam for obtaining Leith holograms. For this system it has proved possible to fully reproduce the conditions under which the holograms were made during the reconstruction stage. The light beam travels strictly in the reverse direction, so that most of the aberrations are eliminated.

All of the systems described above for processing holograms from track chambers during the reconstruction stage have the common feature that the three-dimensional information on the particle tracks and on the event in the track chamber is analyzed by means of traditional imaging optics. When the resolution is high, only a thin layer of the three-dimensional volume being analyzed is clearly visible, and as the depth of focus increases the resolution of the observation system worsens considerably. The problem which had been solved during the stage at which the hologram was made reappeared during the image-reconstruction stage. The questions naturally arise of whether or not the constraints imposed by the traditional imaging optics in the reconstruction stage can be eliminated and whether or not there are completely different methods of solving the depth-of-focus problem. One such method by which this problem can be solved is described in Sec. 2.

2. THE INTENSITY HOLOGRAM FOR PARTIALLY COHERENT ILLUMINATION

The second method of solving the depth-of-focus problem is based on the intensity hologram with incoherent or partially coherent illumination. If the illumination is spatially incoherent, the interference picture produced by the reference wave and the light wave scattered by individual elements of a particle track becomes blurred and its contrast vanishes. This is a consequence of the fact that a monochromatic light source has a large spatial extent, so that the partial interference pictures add with random phases. Nevertheless, even under such unfavorable conditions it is possible to obtain a hologram in the form of an interference picture.

In order to understand the basic principles of this new type of hologram, we consider an object corresponding to a single element of a particle track. A stationary interference pattern can be created if a light wave diverging from this object passes through a beam splitter. This creates two diverging light waves, which are coherent with each other and can form a hologram in the region where they intersect.

The light waves coming from two pointlike light sources, the original object 1 and its virtual image 1′ (Fig. 5), form an interference pattern which is recorded on the hologram.

The structure of the 1–1′ interference pattern is determined by how the light wave from an element of a particle track is split into two parts by the beam splitter. If the track element 1 and its virtual image 1′ lie on the normal to the plane of the hologram, a Fresnel-transform hologram is recorded. On the other hand, if the track element 1 and its virtual image 1′ lie in a plane parallel to the plane of the hologram, a Fourier-transform hologram is recorded. The 1–1′ interference pattern takes the form of a one-dimensional sinusoidal lattice in a plane, i.e., it consists of nearly straight, equidistant bands. A special feature of the interference picture obtained by transverse displacement of the virtual image of the track element is that it contains no information about the distance to the object. However, if the particle track consists of two elements 1 and 2, four diverging light beams are produced. Then the interference pattern contains six components, of which the cross components 1–2, 1–2′, 1′–2, and 1′–2′ blur, since the light source is large. Only two components of the interference pattern remain in the hologram: 1–1′ and 2–2′. No phase information is recorded in this hologram. It is therefore referred to as an intensity hologram.

In order to obtain a Fourier-transform (intensity) hologram of a complex object composed of a large number of particle-track elements, the beam splitter must not only perform amplitude splitting of the light wave incident on it, but must also rotate the original object by an angle of 180° in the plane parallel to the plane of the hologram.

In one of the first studies on intensity holograms,[44] a scheme for obtaining a Fourier-transform hologram was realized. Schemes for obtaining Fresnel-transform holograms were studied in Ref. 45, and in Ref. 47 it was proposed that a triangular interferometer and an afocal optical system be used for this purpose. In Ref. 46 it was pointed out that each point of the object creates a one-dimensional sinusoidal lattice on a Fourier-transform hologram. The spatial frequency and orientation in the plane of the hologram uniquely determine the location of each point of a flat two-dimensional object. During the reconstruction stage the Fourier-transform hologram is illuminated by a spatially coherent converging light beam and the reconstructed image of the flat object is observed within the higher orders of the diffraction pattern.

An intensity hologram obtained with light of wavelength λ_1 must be illuminated during the reconstruction stage by light of wavelength $\lambda_2 = \lambda_1/2$. Otherwise, the image will be reconstructed on a distorted scale. The pattern of illumination which is observed in the reconstructed image corresponds to the square of the intensity in the original object.

In Fig. 6 we show an optical scheme for obtaining a Fourier-transform hologram.[46] An extended, spatially incoherent light source S is transferred by a lens L_1 to a flat object O. The field lenses L_2 and L_3 are aligned such that the central rays from the light source S intersect in the plane of the hologram IH. The system for producing two mutually coherent light beams rotated relative to each other by an angle of 180° consists of a half-silvered mirror BS, a mirror M, and four prisms. The half-silvered mirror BS and the mirror M create two light beams which travel in the vertical direction. The first of these falls on the set of prisms $Pr_1 + Pr_2$, which rotates it to the right, and the second falls on the set of prisms $Pr_3 + Pr_4$, which rotates it to the left. The image of the object at the exit of the prism Pr_2 is oriented at an angle of $+90°$ relative to the original object, and the image at the exit of prism Pr_4 is oriented at an angle of $-90°$ relative to the object. As a result, the intensities of the two images of the

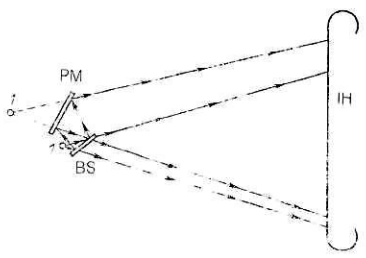

FIG. 5. Scheme for obtaining an intensity hologram of a point object 1: 1′—its virtual image; C—beam splitter; PM—plane mirror; IH—intensity hologram.

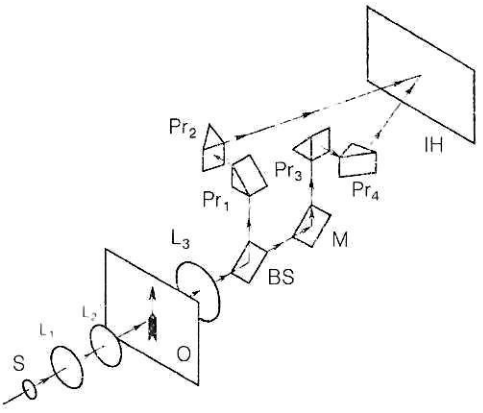

FIG. 6. Scheme for obtaining a Fourier-transform hologram of a flat object O: S—source of a spatially incoherent light beam; L_1, L_2, and L_3—converging lenses; BS—beam splitter; M—mirror; Pr_1, Pr_2, Pr_3, and Pr_4—90° prisms; IH—intensity hologram.

object, which mirror each other relative to a certain point, are related as

$$I(\xi) = I(-\xi). \tag{3}$$

where $\xi(\xi, \eta)$ is a point in the plane (ξ, η). Then the Fourier transforms of two light waves coming from the original pointlike track element $\delta(\xi - \xi_i)$ located at the point ξ_i are

$$\left.\begin{aligned} T_+(\omega) &= \int \delta(\xi - \xi_i) \exp(-i\omega\xi)\, d\xi = \exp(-i\omega\xi_i); \\ T_-(\omega) &= \int \delta(\xi_i - \xi) \exp(-i\omega\xi)\, d\xi = \exp(i\omega\xi_i), \end{aligned}\right\} \tag{4}$$

where $\omega(\omega_x, \omega_y)$ is a point in the plane of the hologram. The coherent superposition of the two light waves $T_+(\omega)$ and $T_-(\omega)$ in the plane of the hologram gives a field of amplitude

$$u_i(\omega) = \exp(i\omega\xi_i) + \exp(-i\omega\xi_i) = 2\cos\omega\xi_i = 2\cos\frac{2\pi}{\lambda l}\mathbf{x}\xi_i. \tag{5}$$

where $\mathbf{x}(x, y)$ is a point in the plane of the hologram, with the coordinate axes x and y related to the coordinate axes ξ and η as

$$\mathbf{x} = \frac{\lambda l}{2\pi}\omega. \tag{6}$$

The distribution of the light intensity in the plane of the hologram is given by the expression

$$I_i(\mathbf{x}) = |u_i(\mathbf{x})|^2 = 4\cos^2\frac{2\pi}{\lambda l}\mathbf{x}\xi_i = 1 + \cos\frac{2\pi}{\left(\frac{\lambda}{2}\right)f}\mathbf{x}\xi_i. \tag{7}$$

From (7) we see that the effective wavelength of the light, $\lambda_{\text{eff}} = \lambda/2$, is half the true wavelength λ. This causes the resolving power of a Fourier-transform hologram to be twice that of a Fourier-transform hologram with coherent illumination for the same hologram aperture.

During the reconstruction stage the Fourier-transform hologram is illuminated by a converging light beam by means of a lens whose focal length is equal to the distance from the object plane to the hologram plane. However, such a hologram actually contains no information on the distance to the object, so that, in principle, the focal length of the lens forming the converging beam during the reconstruction stage is arbitrary. The scale of the image is changed accordingly.

The properties of Fourier-transform holograms with incoherent illumination described above have been used by the authors of Refs. 48–50 and 52 to record simulated particle tracks in track chambers. This was a fundamentally new approach to solving the problem of the depth of focus.

In Ref. 48 it was shown that if the diameter of a particle-track element d is nonzero, then to obtain a Fourier-transform hologram the object must be illuminated by partially coherent light whose spatial-coherence radius satisfies the condition

$$d < l_0 < |r_{ik}|, \tag{8}$$

where r_{ik} $(i \neq k)$ is the radius vector joining two different elements of the particle track. It is only in this case that one obtains a light wave produced by a system of independent sources.

The essence of the method proposed in Refs. 48–50 and 52 is as follows. The illumination of an object by spatially incoherent or partially spatially coherent monochromatic light gives rise to scattered radiation which is partially coherent, and the spatial-coherence function is equal to the Fourier transform of the transmission coefficient of the object.[48,49,51] This function is recorded by means of the interferometer shown in Fig. 6.

In Ref. 48 it was shown that information on the distance, which is contained in the phase of the spatial coherence function, disappears, and the effect of aberrations is canceled at a depth given by

$$\Delta z_{\text{pc}} = \frac{1}{4 \cdot 0.61^2}\frac{d^2}{\sin^2\theta}, \tag{9}$$

where θ is the angular size of the object. This is $\varkappa$,

$$\varkappa = \frac{d}{\lambda \sin\theta \cdot 0.24}, \tag{10}$$

times larger than the depth of focus in the traditional imaging optics with spatial resolution $\Delta x = d$. For $d = 10\,\mu$m the gain is 100:1, but it decreases as d decreases.

In order to retain the information about the spatial location of the particle-track elements, the scattered light is recorded from two different angles using two interferometers (Fig. 6), either with one[48] or with two illuminating light beams. Fourier-transform lenses are used in the schemes shown in Fig. 7. This makes it possible to eliminate the astigmatism at the edges of the image field, which arises if a converging light beam which was absent in the recording stage is used in the reconstruction stage. At the same time the useful depth of focus is increased. In Ref. 50 it was noted that the fully developed method of Fourier-transform holography with partially coherent illumination is less sensitive to the optical nonuniformities created by turbulence of the liquid

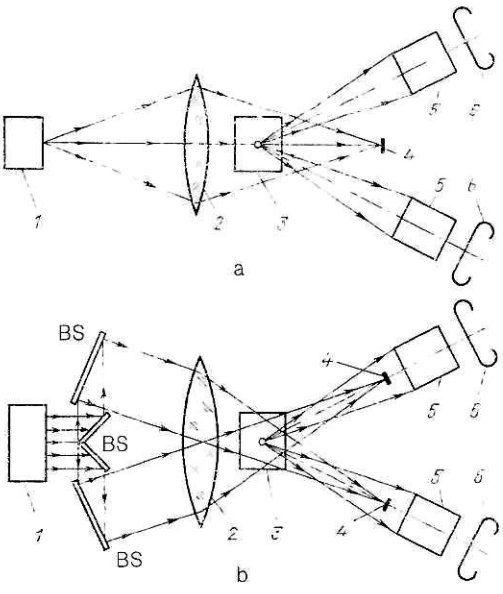

FIG. 7. Stereoscopic schemes for recording two Fourier-transform holograms: a—with a single common converging light beam; b—with two crossed converging light beams. 1—laser; 2—Fourier-transform lens; 3—chamber volume; 4—direct-beam filter; 5—interferometer (see Fig. 6); 6—Fourier intensity hologram.

in the working volume of the track chamber and that it gives a higher contrast in the reconstructed image than in classical holography. The modeling experiments of Refs. 48 and 49, in which glass fibers of diameter 16 μm and light with spatial-coherence radius 20 μm were used, confirmed all the predictions of the fully developed theory of this new method of solving the depth-of-focus problem.

3. THE OBJECTIVE WITH ANNULAR APERTURE

In ordinary photography the problem of the depth of focus is solved very simply. For this it is sufficient to decrease the relative aperture of the objective of the photographic apparatus. For example, for an objective of focal length 58 mm the depth of focus at a distance of 1 m is 97–103 cm (6 cm) for a stop of 1:2 and 77–145 cm (68 cm) for a stop of 1:22. The fact that the diffraction resolution worsens by a factor of 11 is usually not noticed, since neither the film nor the object contains fine detail. The technique of setting the f-stop was used earlier for track chambers, when the size of a particle-track element was 2–3 mm. However, in the current miniature track chambers used to record particle-track elements of dimension 10 μm it is impossible to use the aperture-adjustment technique, because it unavoidably worsens the spatial resolution of the system by an intolerable amount.

In order to increase the depth of focus of the imaging optics while preserving the high spatial resolution, it has been proposed that an objective with annular aperture be used.[55,56] The properties of such objectives have been studied earlier.[53,54] In Fig. 8 we show a scheme for an objective with annular aperture: a is the outer diameter of the objective, εa is its inner diameter, and R is the distance between the objective and the image plane (r, θ). We recall that in a classical aberrationless imaging system the function describing the three-dimensional distribution of light $I_0(z, r)$ in the image plane $(z = 0)$ and along the z axis $(r = 0)$ is given by

$$\left.\begin{aligned} I_0(0, \rho) &= A\left[\frac{2J_1(\rho)}{\rho}\right]^2; \\ I_0(\xi, 0) &= A\left[\frac{\sin(\xi/2)}{\xi/2}\right]^2, \end{aligned}\right\} \tag{11}$$

where

$$\rho = \frac{2\pi a r}{\lambda R}; \quad \xi = \frac{\pi a^2 z}{\lambda R^2}; \quad A = \frac{a^4}{\lambda^2 R^2}. \tag{12}$$

In the case of an annular aperture the corresponding functions $I(0, \rho)$ and $I(\xi, 0)$ have the form

$$\left.\begin{aligned} I(0, \rho) &= A\left[\frac{2J_1(\rho)}{\rho} - \frac{2\varepsilon J_1(\varepsilon\rho)}{\rho}\right]^2; \\ I(\xi, 0) &= A\left\{\frac{\sin\left[\frac{1}{2}\xi(1-\varepsilon^2)\right]}{\frac{1}{2}\xi}\right\}^2. \end{aligned}\right\} \tag{13}$$

From (13) we see that if the area of the "pupil" (the shadow-forming disk) is decreased by a factor of $(1 - \varepsilon^2)$, the depth of focus and the required exposure time increase by a factor of $(1 - \varepsilon^2)^{-1}$. As ε increases, the spatial resolution of the objective $\Delta\rho$ also improves. For example, for $\varepsilon = 0.8$ the resolution $\Delta\rho$ is improved by roughly a factor of 2 in comparison with a system with a completely open aperture $(\varepsilon = 0)$.

A more careful analysis of the effects arising in the use of an objective with annular aperture for track chambers leads to the following conclusions.[55,56] The quality of the image of a bubble obtained with an annular aperture depends on the size of the bubble. The larger the bubble, the worse its image is (!). Here the quality of the image deteriorates very rapidly and becomes worse than in a system with a completely open aperture having the same depth of focus. As ε increases, the intensity of the side lobes of the diffraction pattern of a point increases relative to the central maximum. However, the most serious defect of an objective with annular aperture is the fact that the angular field of the system decreases with increasing ε and also that light losses increase strongly. For example, if the depth of focus must be increased by a factor of 100, the intensity of the light which will be admitted by the annular aperture will be 100 times smaller than in the original system with $\varepsilon = 0$. This is one of the many reasons why the objective with annular aperture has not been widely used in track-chamber technology. Below we shall see how mesooptics can be used to eliminate these light losses while preserving a large depth of focus. For this we must abandon the spherical wave fronts of the classical imaging optics and holography and consider conical wave fronts.

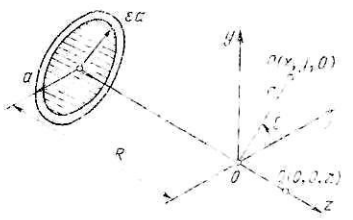

FIG. 8. Objective with annular aperture and the coordinate system: $2a$ is the objective diameter; $2\varepsilon a$ is the diameter of the obstructing disk; R is the distance from the objective with annular aperture to the image plane; $P(x, y, 0)$ is the observation point in the plane $z = 0$; $Q(0, 0, z)$ is the observation point on the axis $x = y = 0$.

4. AXICONS AND MESOOPTICS

Definition

The term "mesooptics"[57] covers a large class of nontraditional imaging systems, in which a pointlike object is transformed into a straight line segment, a circle, an ellipse, a cross, and other complex lines in a plane or in three-dimensional space. The geometrical transformations which are carried out by the mesooptical imaging apparatus can be written as

$$\left.\begin{aligned} &(0-\mathrm{D}) \to (1-\mathrm{D}), \\ &(1-\mathrm{D}) \to (2-\mathrm{D}), \\ &(2-\mathrm{D}) \to (3-\mathrm{D}). \end{aligned}\right\} \tag{14}$$

A point, which is a zero-dimensional (0-D) manifold, is transformed into a straight line segment, i.e., into a one-dimensional (1-D) manifold. A surface, which is a two-dimensional (2-D) manifold, is transformed into part of a three-dimensional (3-D) space. In contrast, in a classical optical imaging system we have transformations of the form

$$(0-D) \rightleftarrows (0-D). \tag{15}$$

This and similar transformations can be regarded as one-to-

one within the approximation of geometrical optics.

There are two main types of mesooptical imaging system[58]: systems with (a) longitudinal and (b) transverse mesooptical properties. Group (a) includes the axicon with a single conical surface, the circular diffraction grating, and the phase-only synthetic hologram with longitudinal mesooptical properties. Group (b) includes the phase-only synthetic hologram with circular response, and also the optical doublet composed of a converging lens and a diverging conical lens. A converging lens combined with a converging conical lens produces two mesooptical images of a point: a longitudinal image on the symmetry axis of the system and a transverse image lying in a plane perpendicular to the symmetry axis of the system. A mesooptical imaging system which transforms a (0-D) object into a two-dimensional (2-D) manifold, for example, in the form of a truncated conical surface, is termed doubly mesooptical: the longitudinal and transverse mesooptical images are formed simultaneously at the same place.

Axicons

The simplest axicon is the conical lens (Fig. 9).[59,60] The focal length in this axicon is

$$L = \frac{a}{2(n-1)\alpha}, \tag{16}$$

where a is the axicon diameter, α is the cone angle, and n is the index of refraction of the glass of which the axicon is made. A conical lens forms a real image in image space and a virtual image in object space. The latter takes the form of a bright ring seen by an observer looking through the conical lens toward the light rays. The useful field of view of a conical lens is very small. It can therefore be used only with coaxially collimated light beams, in scanning systems or in systems with precise alignment.

A circular diffraction grating[61] acts as an axicon whose depth of focus L is given by

$$L^{-1} = 2\lambda/a\delta - l_1^{-1}, \tag{17}$$

where δ is the radius of the circular diffraction grating and l_1 is the distance from the point light source to the circular diffraction grating of diameter a. The radial distribution of the light intensity in the mesooptical image of a point is independent of the light wavelength.

The axicon phase-only synthetic hologram[62] is the holographic equivalent of a lens axicon prepared on a laser reference photograph.[63] Two types of axicon phase-only synthetic hologram have been made[64]: 1) $\lambda = 0.63$ μm, $a = 10$ mm, $L = 2$ m, and $\Delta\rho_{1/2} = 20$ μm, with the distance from the phase-only synthetic hologram equal to 1.6 m; 2) $\lambda = 0.63$ μm, $a = 100$ mm, $L = 50$ m, and $\Delta\rho_{1/2} = 35$ μm, with the distance from the phase-only synthetic hologram equal to 19 m.

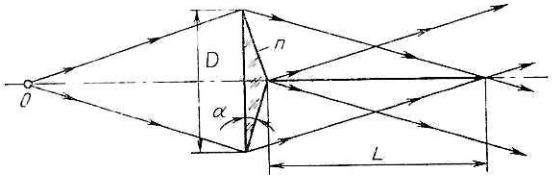

FIG. 9. A conical lens—the simplest axicon: D is the axicon diameter; α is the cone angle; L is the length of the focal line; n is the index of refraction of light in glass.

Axicon doublets and triplets

A converging lens combined with a converging or diverging conical lens[65] produces an image of a point in the form of a focal ring (Fig 10) the radius of which is

$$R_0 \cong (n-1)\alpha F \quad (\alpha < 10^\circ), \tag{18}$$

where F is the focal length of the converging lens. If a mesooptical doublet of this type is illuminated by a Gaussian light beam, the diffraction pattern in the focal ring is described by a Gaussian function whose width is 1.65 times larger than the width of the Gaussian crossover formed near the focus of the positive lens by itself.

Two complementary axicons, one diverging and the other converging, form an analog of the Galilean telescope[66] (Fig. 11). A collimated beam of light in the form of a continuous disk is transformed by this system into a ring-like beam with magnification[65]

$$M \approx 1 - \frac{4\alpha\xi}{a}\left(\frac{n-1}{1-\alpha}\right) \quad (\alpha < 10^\circ), \tag{19}$$

where ξ is the distance between the two complementary axicons. A radial transformation of the wave front is produced by two conical lenses oriented toward each other, or by a conical lens with a plane mirror.[67]

Focusers

This is a new class of optical elements which produce a focal line of arbitrary form.[68,69] The first stage in the construction of a focuser is the solution of the inverse problem[70]: finding the scalar wave field in the plane of the focuser which is transformed into an arbitrary given line with a given distribution of the light intensity in the image plane. The solution of this problem has been found in the geometrical-optics approximation, where the phase of the light field varies slowly over a wavelength λ. This corresponds to the class of mesooptical elements with small relative aperture. Focusers usually have only a phase profile[69] given on some closed two-dimensional region in the plane of the focuser. This region is

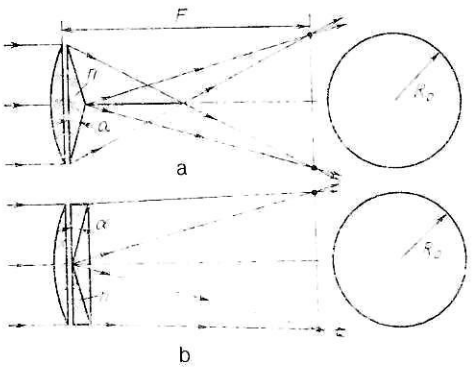

FIG. 10. Lens plus axicon, forming a circular image of a point: a—using a converging axicon; b—using a diverging axicon; R_0 is the focal-ring radius; α is the cone angle; F is the focal length of the lens; n is the index of refraction of light in glass.

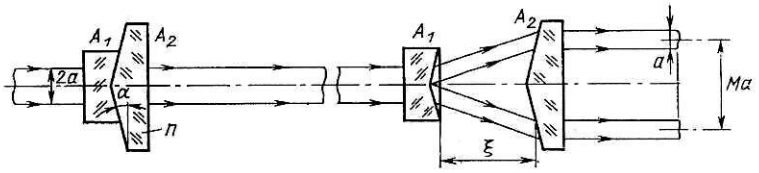

FIG. 11. A system of two complementary axicons A_1 and A_2 for two different axicon positions: $2a$ is the light-beam diameter at the input or ring width at the output.

transformed into the given one-dimensional line in the image plane. Effective algorithms for solving the inverse problems arising in the design of focusers have been developed in the geometrical-optics approximation.[70–72] Smooth single-valued mappings with nonzero Jacobian have been studied.[73] The desired phase profile of the focuser can be specified analytically only in rare cases.[68] The second stage in the design of a focuser is that of obtaining the required optical profile. Precise references and surface etching are used for this. Focusers have been made for light of wavelength $\lambda = 10.6\ \mu$m and $\lambda = 0.6\ \mu$m.[70,72,73] Planar focusers are used in laser ophthalmic surgery for laser keratotomy.[74]

The spherical mesooptical objective

A defect of the axicon and other axially symmetric mesooptical imaging systems is that the angular field of view is very small, owing to the large geometrical-optics aberrations. Such systems can therefore be used only in scanning setups with a point photodetector on the optical axis. However, it is possible to construct a concentric mesooptical system which has an unlimited angular field of view. We recall that the traditional concentric optical objective containing several spherical surface sections with a common center was proposed by Sutton in 1859 (Fig. 12). However, it had no applications in optics, owing to an important defect: the image of points located at the same distance from the center of the concentric objective lies not in a plane, but on a spherical surface. Therefore, for a large angular field of view an image with such characteristics could not be focused and recorded without distortions on flat or cylindrically curved photographic film.

The mesooptical concentric objective behaves differently.[57,75] When the depth of focus of such an objective is sufficiently large, a three-dimensional object can be photographed without distortion on a flat piece of film. In Fig. 13 we show the simplest mesooptical concentric objective with an external spherical surface and an absorbing spherical core.[57,75] The index of refraction of light in the surrounding medium, n_1, differs insignificantly from the index of refraction of light in the spherical layer, n_2. Just like the objective with annular aperture, the mesooptical concentric objective produces good images only of pointlike objects, and not of extended objects. Examples of pointlike objects are the elements of particle tracks in bubble and streamer chambers or the grains of metallic silver of the track of a charged particle in nuclear photoemulsion.

In conclusion, let us return to the question of the basic difference between optics and mesooptics. We note that in a traditional imaging system a spherical wave front diverging from a point source is transformed by an ideal lens into a converging spherical wave front which is recompressed into a pointlike image (Fig. 14). In a mesooptical system, for example, an axicon, a spherical wave front diverging from a point source is transformed into a conical wave front, which produces a mesooptical image of a point in the form of a straight line segment (Fig. 15). Therefore, an imaging device is termed "mesooptical" if it produces conical wave fronts. We recall that undesirable components of conical wave fronts cause aberrations in traditional imaging optics. In particular, aberrations can be chromatic. As a rule, these are undesirable effects which in traditional optics one tries to eliminate by various methods. However, now the situation is different. For example, in Ref. 76 chromatic aberrations were intentionally maximized in order to create a longitudinal spectroscope. A system like this with longitudinal chromatic dispersion should be termed "mesooptical." A point polychromatic light source is transformed by such a system into a straight line segment on the optical axis. It is not impossible that an objective with mesooptical polychromatic properties will be used in a track chamber not only for solving the depth-of-focus problem, but also for preserving distance information.

5. THE MESOOPTICAL FOURIER-TRANSFORM MICROSCOPE FOR NUCLEAR PHOTOEMULSION

The operating principle

The mesooptical Fourier-transform microscope (MFM) (Refs. 77–85) has been designed to search for, observe, and measure the straight tracks of particles in nuclear

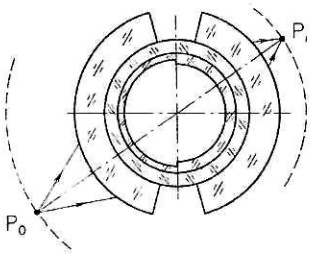

FIG. 12. Transverse cross section of a concentric objective with four spherical concentric surface: P_0—a point object; P_i — its image.

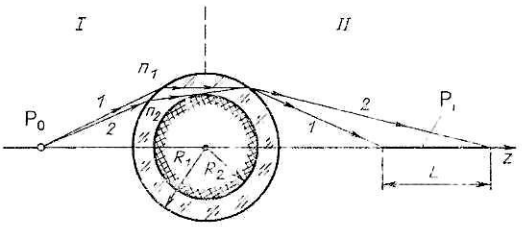

FIG. 13. The simplest mesooptical concentric objective with one spherical surface and absorbing spherical core: P_0—point in object space I; P_i—its mesooptical image in image space II; n_1 is the index of refraction of light in the surrounding liquid; n_2 is the index of refraction of the spherical layer with outer diameter R_1 and inner diameter R_2. The path of extreme rays is shown, and L is the length of the focal line.

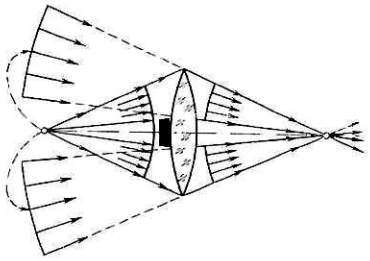

FIG. 14. An ideal lens transforms a diverging spherical wave front into a converging spherical wave front.

photoemulsion which have small dip angles. Information on the spatial location of such objects is preserved in the MFM by means of a type of stereoscopic effect. Therefore, the z coordinate of the center of a straight particle track is measured in the MFM, avoiding the operation of overfocusing in the depth. These and other measuring properties of the MFM have been obtained by the synthesis in a single device of elements of the Fourier-transform optics and the mesooptical principle of image formation.

The MFM contains two basic elements: the Fourier-transformation lens, which produces a converging light beam, and a mesooptical mirror with circular response (Fig. 16). The crossover of the converging light beam occurs at the location of the mesooptical mirror. Light rays diffracted on a straight particle track in nuclear photoemulsion form on the mesooptical mirror a two-dimensional Fourier transform of the straight particle track in the form of a long, narrow band of light, which passes through the optical axis of the MFM and is oriented perpendicular to the straight particle track.

The mesooptical mirror of the MFM has a figure of revolution with generator in the form of an arc of an ellipse.[77] The first focus of the ellipse lies on the optical axis of the MFM in the median plane of the nuclear photoemulsion, and the second focus of the ellipse lies at a distance R from the optical axis in the median plane of the nuclear photoemulsion. If a point light source is placed at the first focus of the ellipse, the geometrical location of the second foci of the ellipse forms a focal ring of radius R_0 (Fig. 16). Owing to diffraction of the light, the focal ring has a finite transverse width which for $\lambda = 0.63\,\mu$m and $R_0 = 80$ mm is $\Delta\rho_{1/2} \approx 1.4$ μm (Ref. 86). The experimentally measured width of the focal ring at the half-max of the light intensity distribution is $\Delta\rho_{1/2}^{\exp} \approx 1.5\,\mu$m (Ref. 86).

The mesooptical mirror of the MFM produces two mesooptical images: one on the left (L) and one on the right

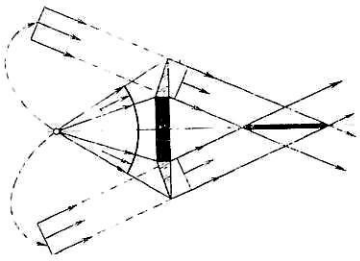

FIG. 15. An axicon transforms a diverging spherical wave front into a converging conical wave front.

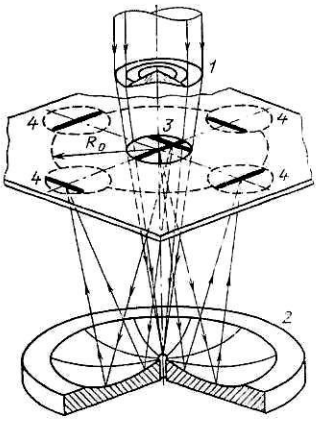

FIG. 16. Optical part of the mesooptical Fourier-transform microscope (MFM), containing a system for producing a convergent light beam 1, a mesooptical mirror with circular response 2, nuclear-photoemulsion layer 3, and a system for observing mesooptical images of a straight particle track 4.

(R). They are located on opposite sides of the focal ring on the line passing through the optical axis of the MFM (Fig. 17). Each mesooptical image of a straight particle track with small dip angle practically touches the focal ring. Mesooptical images of a straight particle track in nuclear photoemulsion are observed and recorded using the matrix of a device with charge coupling in which anamorphic optics is used.[86]

The location of the two mesooptical images of a given straight particle track relative to the central focal ring is determined by three parameters: the angle θ of orientation of the line on which the two mesooptical images of the straight particle track lie, and the apparent distances to the point O of the left (ρ_1) and right (ρ_2) mesooptical images (Fig. 18). Here the distance ρ_0 from the straight particle track to the optical axis and the coordinate z_0 of the center of the straight track are

$$\rho_0 = \frac{\rho_1 - \rho_2}{2\cos\alpha_{1/2}}, \quad z_0 = \frac{\rho_1 + \rho_2}{2\sin\alpha_{1/2}}, \tag{20}$$

where $\alpha_{1/2}$ is the angle between the optical axis of the MFM and the central ray of the diffracted light subtending one half of the mesooptical mirror. A mesooptical mirror of a more complicated shape is used to obtain high spatial resolution in the MFM.[87]

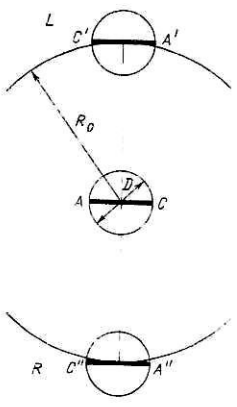

FIG. 17. Relative positions of a straight particle track AC and its two mesooptical images: left ($C'A'$) and right ($C''A''$).

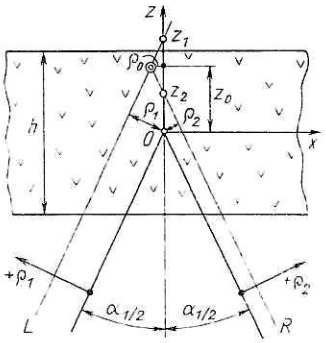

FIG. 18. Transverse cross section of a nuclear-photoemulsion layer with straight particle tracks in the plane perpendicular to a particle track: ρ_1 and ρ_2 are the apparent distances between the particle track and point O for the left and right views, respectively; z_1 and z_2 are the apparent values of the z coordinate of the particle track; ρ_0 is the true distance from the optical axis; z_0 is the true z coordinate of the particle track; h is the thickness of the nuclear-photoemulsion layer; α is the angle between the optical axis and the central ray of diffracted light.

If the straight particle track is located at the edge of the field of view of the MFM, aberrations arise in the mesooptical image. The presence of geometrical aberrations in the meridian cross section of the MFM makes it impossible to decrease the overall dimensions of the mesooptical mirror.[88]

The imaging properties of the MFM in the meridian cross section for a circle, a rectangle, or a half-plane screen can be described using the Dirac delta-plus function $\delta_+(x)$ (Ref. 92) and the spatial Hilbert transform.[93] In the MFM a redistribution of the light intensity occurs which is similar to the effect in W axicons.[94] In Ref. 92 it was shown that the convolution kernel of the MFM has the form

$$g(x)=\frac{d}{dx}[\delta_+(x)], \tag{21}$$

so that an initial quasi-one-dimensional optical field $f_0(x)$ is transformed into the optical signal

$$f(x)=f_0(x)\otimes g(x)=\frac{d}{dx}[\delta_+(x)\otimes f_0(x)]$$

$$=\frac{d}{dx}[f_0(x)+i\chi(x)], \tag{22}$$

where $\chi(x)$ is the Hilbert transform of the function $f_0(x)$ (Ref. 93). The experimental results are in good agreement with this model.[89–91]

In the sagittal cross section the MFM is a one-dimensional pinhole camera with a virtual transmission slit which is always oriented parallel to the straight particle track.[96] There are practically no elements of the imaging optics in this cross section. The width of the transmission slit is equal to the diameter of the crossover of the converging light beam,

$$\Delta\omega \approx \lambda H/l,$$

where H is the distance from the nuclear photoemulsion to the mesooptical element with circular response and l is the length of the straight particle track. Therefore, when the length of the straight track decreases, the virtual diameter of the crossover of the light beam increases (Fig. 19), until it reaches a value equal to the length of the particle track. This occurs when $l=l_0$ and $l_0^2=2\lambda H$. Experiments[96] confirm these predictions.

Measuring characteristics of the MFM

The radial coordinate of a straight particle track ρ_0 and its z coordinate are given by (20), from which we also see that the errors in estimating ρ_0 and z_0 depend on the errors in measuring $\Delta\rho_1=\Delta\rho_2$. The latter are determined by the aperture of half of the mesooptical mirror and in an actual setup are $\Delta\rho_{1/2}\approx 1.5\ \mu$m (Ref. 86).

If the length of the straight particle track l is less than the diameter of the field of view D, the visible orientation angles θ_L and θ_R measured for the two mesooptical images of the particle track determine both the actual angle of orientation of the particle track,[97]

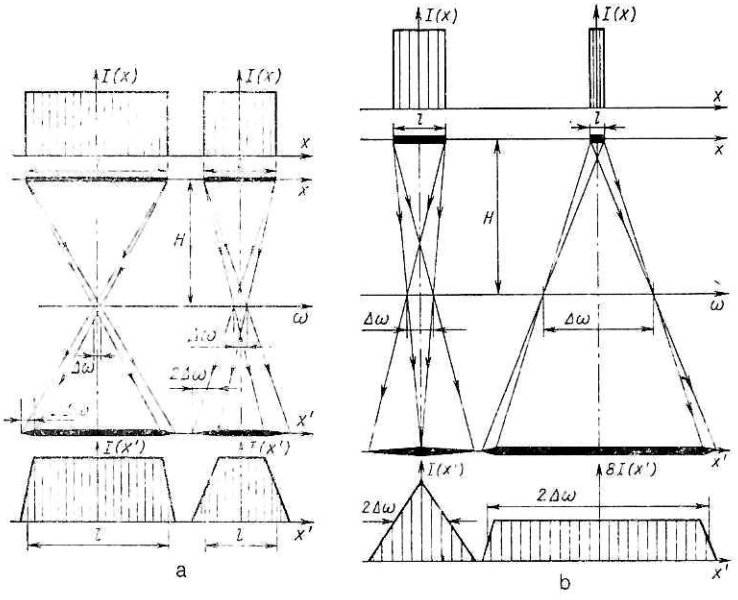

FIG. 19. Mesooptical images of a straight particle track of length l in the saggital cross section of the MFM: a—for $l>l_0$; b—for $l\leqslant l_0$.

$$\theta_0 = \frac{1}{2}(\theta_L + \theta_R), \tag{23}$$

and the length of the straight track l:

$$(\theta_L - \theta_R) = \frac{1}{R_0}(D - l). \tag{24}$$

Since the angles θ_L and θ_R can take both positive and negative values, the length of a straight particle track can be either positive or negative. The observer can thereby estimate the coordinate of the beginning or the end of a straight particle track within the field of view of the MFM. The average error in measuring the track length is about 30 μm. This is quite sufficient for reaching the vertex of a nuclear interaction repeatedly on the basis of data obtained with the MFM.

The mesooptical analog of the Moiré effect is used for precise measurements of small scattering angles and particle decay lengths with the MFM.[98] If the outer end of the right half of the particle track (Fig. 20) is rotated about the center of the field of view in the direction perpendicular to the orientation of the straight particle track, the mesooptical images of this half of the track will move together along the corresponding original mesooptical images, i.e., perpendicular to the velocity vector of the outer end of the right half of the particle track. The linear speed of this motion is R/D times larger than the true speed of the outer end of the right half of the particle track. The same relation is valid for absolute displacements. The error in measuring the particle scattering angle in a "kink" is $\pm 1'$ for $D = 3$ mm, $H = 150$ mm, and $R_0 = 80$ mm. In Fig. 21 we show the scheme for measuring the decay length for the event shown in the upper part of the figure.[98]

The MFM can be used to measure the radius of curvature of a curved particle track.[99] The carrier of this information in the MFM is the length of the mesooptical image. In order to estimate the radius of curvature of a particle track, it is sufficient to measure two linear quantities: the length of the left and right mesooptical images of the given track. The basic principle of this new method of measuring the curvature of a particle track is shown in Fig. 22. The length of the mesooptical images l_L and l_R at the half-max of the light

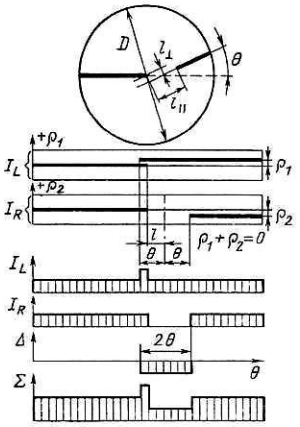

FIG. 21. Scheme for measuring the decay length for the event shown in the upper part of the figure. Bottom—distribution of the light intensity in projections of the mesooptical images on the θ axis: I_L, I_R, $\Delta(\theta)$, and $\Sigma(\theta)$; ρ_1 and ρ_2 are the radial coordinates of the secondary-particle track for the left- and right-hand mesooptical images; $l_\perp$ is the transverse component of the decay length, $l_\perp = |\rho_1| = |\rho_2|$; here the longitudinal component of the decay length $l_\parallel$ is measured using an ordinary microscope.

intensity distribution profile are related to the radius of curvature of the track ρ as

$$l_L/(\rho + R) = l_R/(\rho - R_0), \tag{25}$$

from which

$$\rho = R_0 \frac{l_L + l_R}{l_L - l_R} \cong \frac{2R_0 L}{\xi}, \tag{26}$$

where $\xi = l_L - l_R$ is the length difference. We note that the ratio of the length difference ξ to the curvature $s \cong L^2/8\rho$ is

$$\xi/s = 16R_0/L. \tag{27}$$

For $R_0 = 80$ mm and $L = 1$ mm, $\xi/s = 1.28 \times 10^3$. This means that the length difference ξ is about 10^3 times larger than the curvature s of a curved particle track inside the field of view of the MFM. For example, if $s = 0.1$ μm, then $\xi = 128$ μm or about $0.13 l_{ave}$, where $l_{ave} = (l_L + l_R)/2$.

This new method of measuring the radius of curvature of a curved particle track, which has been studied experimentally in Ref. 99, can be used to measure particle tracks in

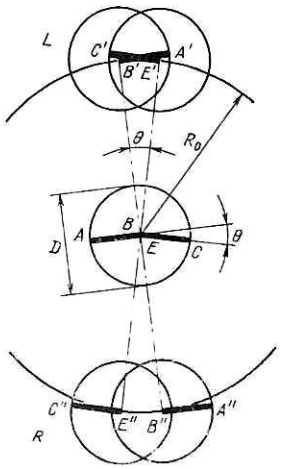

FIG. 20. Mesooptical images of a kink type of event, consisting of two particle tracks AB and EC with a small angle θ between them: top—left-hand mesooptical image; bottom—right-hand image; R_0 is the focal-ring radius; D is the diameter of the field of view.

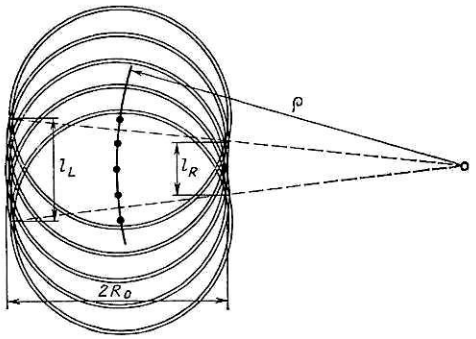

FIG. 22. Basic principle for measuring the curvature of a particle track using the MFM: l_L is the length of the left-hand mesooptical image; l_R is the length of the right-hand mesooptical image; ρ is the radius of curvature of the particle track; R_0 is the focal-ring radius; $\rho > R_0$.

nuclear photoemulsion for the purpose of estimating local deformations of the distortion type and also in track chambers with a magnetic field.

The algorithm for event searches

Use of the MFM allows one to rapidly find a nuclear interaction vertex (an "event"), which is seen as a "star" in the nuclear photoemulsion. The coordinates of the event vertex are found directly from the mesooptical images of straight particle tracks in the MFM output without the stage of track reconstruction in three-dimensional space, as is usually done. The method is based on the fact that both the left and the right mesooptical images of the particle tracks forming an event lie on a sine curve (a "sinogram") in the variables (ρ, θ). This is true even when the event vertex lies outside the field of view or outside the nuclear-photoemulsion layer. In Fig. 23 we show the position of the centers of the mesooptical images of seven straight particle tracks in the (ρ, θ) format. Only six of these come from the common vertex, while the seventh particle track does not belong to this event.

In the tangent algorithm for event searches[100] only those particle tracks which intersect the center of the field of view at a given instant of time are observed and recorded. In Fig. 24 we show a four-prong event and a separate particle track unrelated to the event. The results of the measurements are shown in the (tan θ, x) format, where x is the position of the nuclear photoemulsion at the instant of time when the particle track intersects the center of the MFM field of view for displacement of the nuclear photoemulsion along the x axis at fixed coordinate y_c plotted along the y axis. In the (tan θ, x) format the centers of the mesooptical images lie strictly on a straight line if the corresponding particle tracks have a common vertex. The angle of the slope of a given straight line relative to the axis, tan θ, is $\beta = \tan^{-1}(y_0 - y_c)$, where (x_0, y_0) are the coordinates of the event vertex, and the coordinate x_0 corresponds to the point on the x axis through which a straight line of the event passes in the format (tan θ, x). The smaller the difference $(y_0 - y_c)$, the smaller the angle β.

If the event vertex is located on the optical axis of the MFM, the mesooptical images of the particle tracks of the star lie on one of the focal circles with center on the optical axis. This feature is used in the algorithm of direct detection of an event in the MFM without the stage of observation and recording of the mesooptical images of the individual straight particle tracks forming the event. Since the radius of the focal circle is determined by the z coordinate of the event vertex, the total number of information degrees of freedom along the z axis is

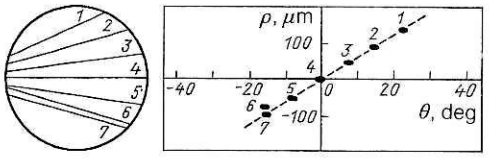

FIG. 23. A picture of seven straight particle tracks in the MFM field of view (left) and their mesooptical images in the format (ρ, θ) (right). Only one of the two mesooptical images is shown.

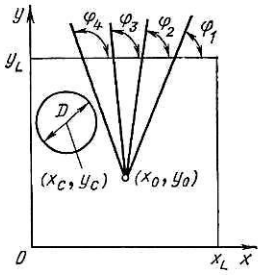

FIG. 24. Tangent algorithm for event searches, for the example of an event with four particle tracks and vertex at the point (x_0, y_0) of a coordinate system rigidly fixed to the nuclear photoemulsion. The center of the field of view of the MFM of diameter D is located at the point (x_c, y_c). The orientation angles of the particle tracks of the event in the (x, y) plane are φ_1, φ_2, φ_3, and φ_4.

$$N_z = \frac{h}{\Delta z} = \frac{h \sin \alpha_{1/2}}{\Delta \rho}, \tag{28}$$

where $\Delta\rho$ is the effective width of the focal ring in the MFM. For $\Delta\rho = 5$ μm, $\alpha_{1/2} = 30°$, and $h = 200$ μm, we have $N_z = 20$. The direct method of recording events in nuclear photoemulsion was demonstrated experimentally on a model MFM (Ref. 101) containing a phase-only synthetic hologram with ring response in the spatial-frequency plane and a system of concentric transmission rings in the plane of the mesooptical images.

Tracks of highly ionizing particles

The role of the mesooptical element with ring response can be played by a system of three axicon lenses (Fig. 25) with conical and spherical outer surfaces.[102,103] This system creates a stereoscopic effect, which can be used to measure the z coordinate of the center of a straight track in the MFM, thereby avoiding the operation of scanning with overfocusing along the z axis. In order to decrease the effective aperture of each half of the mesooptical element with ring response, the construction of the three axicon lenses is changed in the following manner (Fig. 26). System A consists of three annular axicon lenses. System B contains not

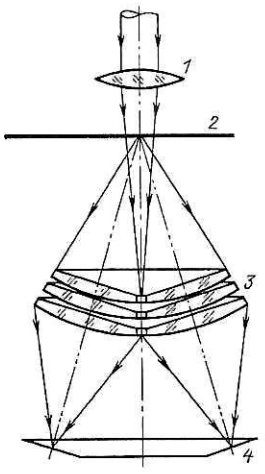

FIG. 25. A mesooptical Fourier-transform microscope with three axicon lenses: 1—Fourier objective; 2—nuclear-photoemulsion layer; 3—a system of three axicon lenses; 4—observation screen.

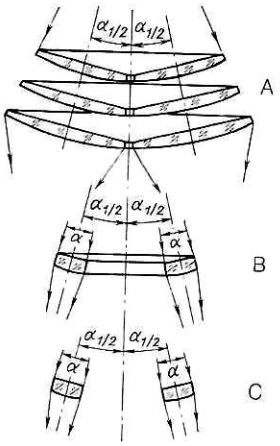

FIG. 26. Construction of several mesooptical elements of the MFM: A—in the form of three circular axicon lenses; B—in the form of a single narrow circular axicon lens; C—in the form of two cylindrical lenses.

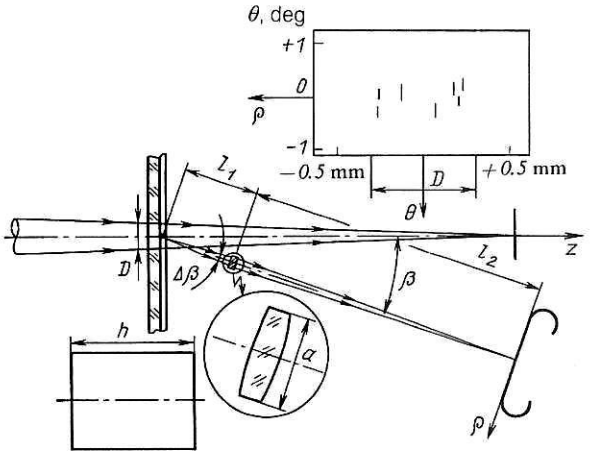

FIG. 27. A mesooptical system with cylindrical lens used to form mesooptical images of quasiparallel particle tracks and the experimental results in the format (ρ, θ): D is the diameter of the field of view; $\Delta\beta$ is the aperture angle of the cylindrical lens of width a in the meridian cross section; h is the length of the straight generating cylindrical lens; β is the observation angle; l_1 is the distance between the particle track in the nuclear photoemulsion and the cylindrical lens; l_2 is the distance between the cylindrical lens and the mesooptical image; ρ is the radial coordinate of the mesooptical image of a straight particle track; θ is the orientation angle of a straight particle track;, $\theta = 0$ corresponds to particle tracks which are strictly perpendicular to the plane of the figure.

three, but one axicon lens in the form of a narrow ring. Finally, system C contains two cylindrical lenses and can be used to observe primary tracks of highly ionizing particles, for example, relativistic neon nuclei, which produce tracks nearly parallel to each other. The mesooptical images of these tracks are effectively formed by a very small segment of the focal circle, $\sim 1°$, which can be approximated by its tangent line. Since the rest of the focal circle is not used, the function of the mesooptical element with ring response can be accomplished by a system of two cylindrical lenses located on opposite ends of the focal circle such that the generator of each cylindrical lens is parallel to one of the highly ionizing particle tracks.

It has been shown in experiments[104] that the size of the mesooptical image in the sagittal cross section of a system with two cylindrical lenses can be decreased considerably if the crossover of the converging light beam is shifted from the spatial-frequency plane to a plane located near the mesooptical images (Fig. 27). Both monocular and binocular stereoscopic effects are observed in such a system.[104] It has been shown that the number of information degrees of freedom in the MFM with a single cylindrical lens is 150 times larger than in the traditional optical microscope with resolution $\Delta\rho = 5\ \mu$m, while an MFM with two cylindrical lenses has additional information degrees of freedom along the z axis ($N_z \approx 18$).

Apodization in mesooptics

Apodization effects in mesooptics arise as a result of the natural screening of the pupil of a mesooptical imaging system. Apodization effects in MFMs have been modeled[95] for three classes of input signals entering one of three types of mesooptical element with ring response: a cylindrical mesooptical mirror and toroidal mesooptical mirrors with and without a cut at the center. The MFM with a toroidal mesooptical mirror produces spatial differentiation along the radial coordinate of a square-wave signal if the width of the pulse is equal to or larger than the MFM resolution along the radial coordinate. The delineation of a square-wave pulse is also observed in a cylindrical mesooptical mirror, but it begins later and gives less of a contrast than in a toroidal mesooptical mirror.

A different picture is observed for the bell-shaped cosine and Gaussian functions. The delineation effect does not arise in any of the three mesooptical systems studied. However, other useful effects appear. For example, a broad Gaussian function describing the reference grid on a nuclear-photoemulsion surface has its intensity suppressed by at least a factor of 362 in a mesooptical mirror with a cut at the center. Here the output signal is close to a Gaussian, and its width is 1.5 times larger than the width of the Gaussian at the output.[95]

The method of measuring the width of a particle track

A straight particle track in nuclear photoemulsion consists of a chain of silver grains randomly distributed in the direction perpendicular to the actual trajectory of the charged particle. Therefore, its profile along the radial coordinate, averaged over some length of the particle track, can be approximated by a Gaussian. Its width is related in a known manner to the speed and mass of the particle. However, as was shown in Ref. 95, the Gaussian function is not distinguished by means of the natural apodization in the MFM. In order to distinguish the Gaussian function and thereby create the conditions for the reliable measurement of the width of the particle track, it is necessary to use the technique of optical-signal differentiation, which is widely used in Hilbert optics.[93]

6. MESOOPTICAL MICROSCOPES FOR VERTICAL PARTICLE TRACKS

The mesooptical scanning microscope

Particle tracks in nuclear photoemulsion which are parallel to the optical axis of the microscope are termed "verti-

cal." For a large increase of the microscope size they are only partially seen. In order to verify that a given vertical track of a particle passes through the entire layer of nuclear photoemulsion, and is not an accidental cluster of silver grains, the operator must constantly change the position of the sharp focus along the z axis. However, this scanning along the z axis can be completely eliminated if the optical microscope is replaced by a mesooptical scanning microscope in which the traditional objective is replaced by a mesooptical axicon and a point photodetector is located on its optical axis (Fig. 28).

The intensity of the side lobes in the smearing function of a point is decreased by means of a multiaxicon, for example, a double axicon with two conical surfaces.[111] The disadvantage of a double axicon is that it produces a longitudinal z modulation of the light intensity on the axis with period

$$\Lambda \approx \frac{\lambda \sqrt{F^2+R^2}}{(\gamma-1)R}, \tag{29}$$

where F is the focal length of the double axicon, $2R$ is the outer diameter, and γ is the ratio of the diameters of the inner and outer axicons. For $\lambda = 0.63$ μm, $F = 150$ mm, $R = 60$ mn, and $\gamma = 0.7$, we have $\Lambda \approx 5.5$ μm. This z modulation does not interfere with the observation of vertical particle tracks of length 200 μm. However, when the z modulation is undesirable, it can be smoothed out by means of a phase plate, which is placed near the double axicon. Its dimensions are such that the phase plate covers only the light rays coming from the inner axicon. The phase plate is divided into N sectors ($N \geqslant 2$).[111] The phase shift in each sector is $(360°/N)(k-1)$, where k is the index labeling the sector, $k = 1, 2, \ldots, N-1, N$. Such a phase plate produces a longitudinal shift of the wave-field components in a given sector by an amount $(\Delta/N)(k-1)$, as a result of which the contrast from the z modulation of the light nearly vanishes.

An even higher efficiency can be obtained by using the multichannel mesooptical microscope,[105] which contains a two-dimensional block of prisms, a screen with a two-dimensional regular block of apertures, a photodetector, and a spherical mesooptical objective[57] (Fig. 29). A vertical particle track is observed in parallel light rays, and the recording is made in light rays which are homocentric and pass through the center of the spherical mesooptical objective. One system of rays is transformed into the other by means of a two-dimensional block of N^2 prisms with a square base, where N is an odd number, $N \geqslant 3$. Each aperture in the screen is located on the light beam which comes from the center of the corresponding square prism. The nuclear photoplate is shifted within the region of one square prism of area a^2, where a is the length of a side of the base of the square prism. Since there are many channels, the system actually scans a region of the nuclear photoemulsion of area N^2a^2. The distance between successive positions of the nuclear photoemulsion is Na along the x and y axes. The coordinates of a detected vertical particle track (x, y) are determined by the coordinates of the nuclear photoemulsion at the time the measurements are made, and also by the indices m_x and m_y of the aperture in the screen through which the rays of diffracted light have passed.

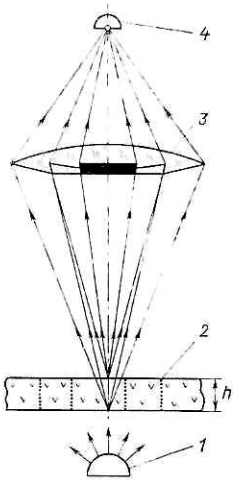

FIG. 28. A mesooptical scanning microscope with a double axicon: 1—light source; 2—nuclear-photoemulsion layer; 3—double axicon; 4—point photodetector; h is the thickness of the nuclear-photoemulsion layer.

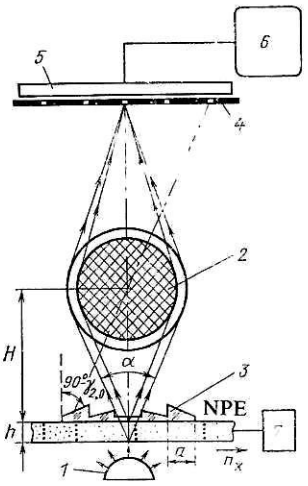

FIG. 29. A multichannel mesooptical scanning microscope: 1—light source; 2—spherical mesooptical objective; 3—prisms with square base; 4—screen with two-dimensional array of point apertures; 5—photodetector; 6—screen; h is the thickness of the nuclear-photoemulsion layer; H is the distance between the center of the spherical mesooptical objective and the nuclear photoemulsion. The dashed line shows a light ray coming from the center of the prism with indices $m_x = 2$ and $m_y = 0$ at an angle $90° - \gamma_{20}$ to the optical axis of the system; NPE—nuclear photoemulsion.

The mesooptical confocal microscope

The traditional optical confocal microscope[106–109] contains two objectives, an illuminating objective and a collecting objective, and also a photodetector with a point aperture (Fig. 30). The axial scanning of a three-dimensional object is carried out at sound frequencies, and the transverse scanning along the x and y axes is performed using an ordinary mechanical system. The image of an object, for example, the nonplanar wing of an insect, is formed on a visual display screen. The noteworthy feature of the confocal microscope is that the coherent smearing function of a point in the confocal microscope is equal to the product of the corresponding coherent smearing functions for each objective. Therefore, the side lobes of the smearing function of a point are so weak

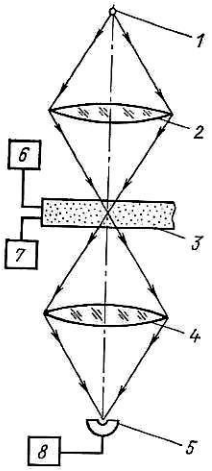

FIG. 30. The traditional optical confocal microscope: 1—point light source; 2—illuminating objective; 3—object; 4—collecting objective; 5—point photodetector; 6—system for scanning along the z axis; 7—system for scanning along the x and y axes; 8—observation screen.

that the system permits summation over the intensities of many partial images for different z without weakening the contrast and without decreasing the signal-to-noise ratio in the sum image.

Axial scanning along the z axis is completely absent in the mesooptical confocal microscope[110,111] (Fig. 31). Each objective of the mesooptical confocal microscope consists of a collimator lens and a multiaxicon. In order to preserve the confocal topology of the path of a light ray in the mesooptical confocal microscope, it is necessary that the light rays in the space between the two multiaxicons be parallel in the meridian cross section for each pair of axicons facing each other. In order to eliminate the longitudinal light modulation arising from the multiple-wave propagation of the light, the absolute dimensions of each muiltiaxicon are increased without changing the initial aperture. For example, if the distance from the multiaxicon to the nuclear photoemulsion is increased to 100 mm, the period of the z modulation of the light in the vicinity of the focal point is

$$\Lambda \approx \frac{\lambda H}{h \sin \frac{\alpha}{2}} = 630\,\mu\text{m} \qquad (30)$$

for $h = 200\,\mu$m and $\sin(\alpha/2) \approx 0.5$.

The mesooptical condenser

The speed of operation of a system for detecting vertical particle tracks in nuclear photoemulsion is increased further by eliminating the operation of displacement along the y axis. For this purpose, the mesooptical condenser[111] (Fig. 32) is introduced into the traditional optical microscope. This condenser consists of a source of a collimated light beam and a cylindrical mesooptical lens whose generating element is a polygon.[112] It can be viewed as a one-dimensional analog of a multiaxicon with many conical surfaces. An interference pattern of period $d = \lambda/(2\sin(\theta/2))$ is formed at the intersection of two plane waves arriving from two elementary prisms located at angles of $+\theta/2$ and $-\theta/2$ to the symmetry plane of the system. The interference patterns created by the several pairs of elementary prisms of a cylindrical mesooptical lens add constructively at the location of the central maximum. The width of an elementary prism is

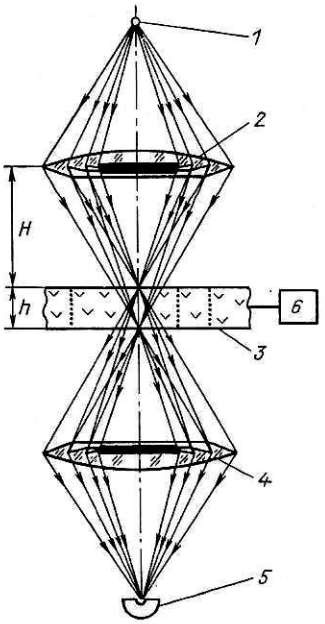

FIG. 31. The mesooptical confocal microscope: 1—point light source; 2—illuminating objective–multiaxicon; 3—nuclear photoemulsion; 4—collecting objective–multiaxicon; 5—photodetector; 6—system for scanning along the x and y axes; h is the thickness of the nuclear-photoemulsion layer; H is the distance between the objective–multiaxicon and the nuclear photoemulsion.

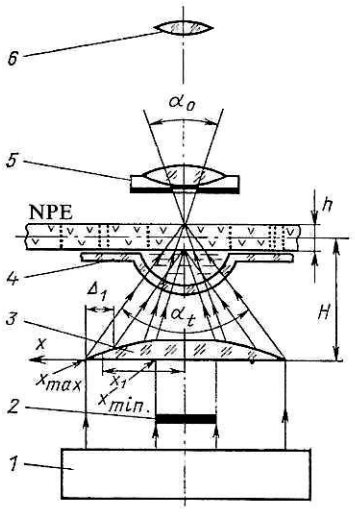

FIG. 32. Microscope for vertical particle tracks containing a mesooptical condenser: 1—collimated light beam; 2—screen; 3—mesooptical cylindrical lens with generator in the form of a polygon; 4—cylindrical immersion bath; 5—microscope objective; 6—microscope eyepiece; $2x_{max}$ is the total width of the mesooptical cylindrical lens; $2x_{min}$ is the total width of the screen; Δ_1 is the width of the first, outer, elementary prism, located a distance x_1 from the symmetry plane; H is the distance between the mesooptical cylindrical lens and the nuclear photoemulsion; α_t is the total angular aperture of the mesooptical cylindrical lens; α_0 is the aperture of the microscope objective for observing vertical particle tracks; h is the thickness of the nuclear-photoemulsion (NPE) layer.

$\Delta = xh/H$. The resolving power of the mesooptical condenser is $\lambda/\alpha_{\text{eff}}$, where α_{eff} is the effective aperture of the mesooptical condenser, which is always smaller than the pole aperture α_t. For $H = 100$ mm, we have $\alpha_t = 0.58$ rad and $\alpha_{\text{eff}} = 0.33$ rad. The spatial resolution of a mesooptical condenser of these dimensions is $\Delta\rho_{\text{eff}} \approx 2$ μm.

When a vertical particle track is made in an illuminated region of width 2 μm, the light diffracted on this particle track reaches an objective with numerical value of the aperture $\alpha_1 = \sqrt{2\lambda/h} = 0.08$ rad from the entire length h.

The x and y coordinates of a vertical particle track are measured using an algorithm borrowed from reconstructive tomography.[113] The nuclear-photoemulsion layer with vertical particle tracks is scanned twice, each time along the x axis, but for different orientations of the narrow illuminated region relative to the x axis. For orientation angles of $+45$ and $-45°$, the x and y coordinates of a vertical particle track are found from the equations

$$2x = x_1 + x_2; \qquad 2y = x_1 - x_2, \tag{31}$$

where x_1 and x_2 are the position coordinates of the nuclear photoemulsion at the instant of time that the vertical particle track is located inside the narrow illuminated region. If the number of vertical particle tracks in the field of view of the system is $N > 1$, then the number of independent orientations of the narrow illuminated region relative to the x axis must be increased to $2N$. The expected scanning rate for nuclear photoemulsion using the mesooptical condenser is 10–20 mm^2/sec.

CONCLUSIONS

Let us now compare the possibilities and limitations of the methods described above for solving the problem of the depth of focus. First of all, we note that mesooptics has the most favorable characteristics in comparison with traditional imaging optics or holography, and it allows the construction of systems which, after specialization, will be the most capable of meeting the requirements of high-energy physics. There is every reason to expect that mesooptics will breathe new life into the track-detector method. Most mesooptical systems are considered specialized, because mesooptics offers important advantages over classical imaging optics only for a narrow class of objectives consisting of a chain of point-like elements. The use of mesooptics outside this class of objects is generally not advantageous. However, the range of applicability of a number of mesooptical setups can be broader than suggested above. For example, the mesooptical Fourier-transform microscope is at the same time a new type of tomographical device.

The classical photographic objective

In science and technology, the classical photographic objective is traditionally used universally for the observation and photographing of a very large class of objects. In high-energy physics, the classical photographic objective is encountered in the photographic recorders of track chambers, in microscopes for observing particle tracks in nuclear photoemulsion, and in scanning systems. The drawback of the classical photographic objective is the fact that its resolving power in the transverse direction, Δx, is uniquely related to the imaging depth of focus Δz:

$$\Delta x = \sqrt{2\lambda\Delta z}. \tag{32}$$

Therefore, the classical objective cannot be used for photographing track elements of diameter $d = 5$ μm in a track detector of depth $\Delta z = 100$ mm.

The wave field hologram

For recording events in a track chamber of depth Δz it is sufficient that the degree of monochromaticity of the radiation of a single-mode laser, $\lambda/\Delta\lambda$, satisfies the relation

$$\frac{\lambda}{\Delta\lambda} > \frac{\lambda\Delta z}{12\,d^2}. \tag{33}$$

Since the relative shading of the track chamber by particle tracks is usually small, wave-field holograms are usually obtained using the Gabor scheme, or a focused-image hologram is made. An important deficiency of the wave-field hologram is that during the reconstruction stage one must use the traditional imaging optics with all its limitations. These can be eliminated if the classical photographic objective is replaced by a mesooptical imaging element whose depth of focus has the required constant or adjustable value for high resolution in the transverse direction.

The intensity hologram

This solves the depth-of-focus problem, but only partially. For example, for $\Delta x \gtrsim 5$ μm the depth of focus increases by at least a factor of 100, but for $\Delta x \lesssim 1$ μm the depth of focus is only slightly larger than that of the classical photographic objective. An important advantage of the intensity hologram is that the reconstructed image has a high contrast in the intensity. In photography this corresponds to $\gamma = 2$, which is usually attained with a small decrease of the light intensity on the object in a certain mode of developing the photographic film. The second advantage of this method is that planar images, as in ordinary stereoscopy, are obtained in the reconstruction stage. The existing systems of processing film information are suitable for analyzing them. Mesooptics is not required. The defect of the intensity hologram is that, owing to the high level of incoherent background, the charging of the track chamber by the beam particles will be considerably smaller than allowed by the wave-field hologram.

Objectives with an annular aperture

For a large depth of focus, the light-collecting efficiency and also the angular field of view are very small. The latter problem can be solved if the size of the objective with annular aperture is many times larger than the size of the classical photographic objective. Finally, the intensity of the side lobes in the smearing function of a point is large, and their falloff with distance from the center of the image is slower than for a classical aberrationless photographic objective. This significantly decreases the dynamical range of the system. Therefore, objectives with an annular aperture have hardly been used at all.

Mesooptical imaging systems

The light-collecting efficiency is only somewhat higher than for the classical photographic objective, but it is consid-

erably higher than for the objective with annular aperture. However, the angular field of view is just as small as for the objective with annular aperture. The problem of the side lobes is partially solved by using multiaxicons. The spherical mesooptical objective has unique properties. However, here the problem of the immersion bath has not been solved, and the optimal construction of the spherical mesooptical objective has not been found. Nevertheless, it can be stated that it will have many applications in track chambers, in the nuclear-photoemulsion technique, and in systems for observing events reconstructed by means of holograms.

The mesooptical Fourier-transform microscope

This is a specialized system for seeking particle tracks with small dip angle. The operating speed is very high: in the MFM there is no depth-scanning stage, and the information on the spatial location of a particle track has a compact form, not being split up according to the individual elements of the particle track. Finally, the identification of direct particle tracks is done almost instantaneously in the MFM using a coherent light beam. This is possible because the mesooptical mirror of the MFM has a complicated surface of revolution, and its dimensions are many times larger than any traditional microscope objective.

The mesooptical Fourier-transform microscope as a new type of tomographical device

As is well known, a tomogram is an image of the internal structure of a three-dimensional object in a two-dimensional slice obtained without harming the object. In order to obtain a tomogram, the object is x-rayed in a thin slice at a large number of different angles, and the resulting data are processed using the inverse Radon transformation. A tomogram can reveal the distribution of the density of a given type of nucleus, the elastic characteristics of a medium, anatomical or biochemical parameters, and the velocity field of a fluid. Tomograms obtained using the MFM have certain special features. First, the MFM "sees" only linear objects with a small dip angle. Second, the MFM tomogram consists of a set of bright points on a dark field. Each point corresponds to the location of the intersection of the tomogram plane by a linear object moving at an angle of 90° with respect to the tomogram plane. All the other linear objects moving at other angles to the tomogram plane are not visible in this tomogram. The resolution in the orientation angle of a linear object is at least 5′. Here there is no inverse-transformation stage. Each nuclear photographic plate with charged-particle tracks has dimensions $200\times100\times0.2$ mm. The total number of resolution elements on one such photographic plate is 1.6×10^{12} bits, which is equivalent to 2×10^{7} traditional tomograms with 256×256 image elements.

Mesooptical microscopes for vertical particle tracks

These have been designed for the rapid search for vertical particle tracks in nuclear photoemulsion. The operation of scanning along the z axis, which is unavoidable in classical and traditional confocal microscopes, has been completely eliminated here, and the problem of the side lobes of the smearing function of a point, which is typical of any imaging system with an annular aperture, has also been solved.

The mesooptical condenser has unique features. Of the three scanning operations along the x, y, and z axes necessary in the traditional optical microscope, here only displacements along the x axis remain. In order to obtain complete information on a vertical particle track, it is sufficient to scan along the x axis two times for different positions of the mesooptical condenser relative to the x axis.

Where should mesooptics be used?

Mesooptics is suitable for use in holography during the stage of reconstruction, observation, and readout of nuclear-interaction images, and also in traditional systems for scanning and measuring events in photographs obtained in track chambers with a magnetic field. The latter possibility arose after it was shown theoretically and experimentally that the MFM allows the operational measurement of the radius of curvature of a particle track. In order to use the MFM in a traditional system for scanning and measuring events, it is necessary to incorporate an additional inverse microscope which decreases the field of view of the system. In a system composed of these three elements the ratio of the diameter of the focal circle and the diameter of the field of view will be large, while the overall size is small. Finally, it is advantageous to replace the classical photographic objective by a mesooptical objective in track chambers where the charging by primary particles of the beam is small.

Conclusions

Mesooptics is now being studied theoretically and experimentally using mock-up systems or real operating mesooptical elements. The technical problems of making a mesooptical mirror with circular response of diameter 160 mm and spatial resolution 1.5 μm have been solved successfully. However, at present there is still no mesooptical device which operates on-line with a computer. We can therefore speak only of the potential possibilities of the mesooptical systems discussed in this review. In particular, we recall that the high operating speed of the mesooptical Fourier-transform microscope for nuclear photoemulsion is a consequence of the fact that here the universal optical microscope is replaced by a specialized system composed of objects from a tiny class. This allows the elimination of the operation of depth scanning in the nuclear-photoemulsion layer, while preserving the information on the z coordinate of a straight particle track.

It has recently been shown that the overall dimensions of mesooptical elements can be decreased. It has also been found experimentally that the mesooptical Fourier-transform microscope for nuclear photoemulsion can be used to see not only straight particle tracks with small dip angle, but also straight particle tracks forming an angle of 30–40° to the plane of the nuclear photoemulsion. Finally, there is every reason to expect that the class of elements which can be observed and studied using mesooptics will continually grow.

[1]A. P. Komar, M. V. Stabnikov, and B. G. Turukhano, Dokl. Akad. Nauk SSSR **169**, 1052 (1966) [Sov. Phys. Dokl. **11**, 712 (1967)].
[2]A. P. Komar, M. V. Stabnikov, B. G. Turukhano, and N. Turukhano, Preprint No. 079 [in Russian], Physicotechnical Institute, USSR Academy of Sciences, Leningrad (1968).
[3]L. M. Soroko, Fiz. Elem. Chastits At. Yadra **3**, 688 (1972) [Sov. J. Part. Nucl. **3**, 352 (1972)].

[4]M. V. Stabnikov and M. Sh. Tombak, Zh. Tekh. Fiz. **42**, 1073 (1972) [Sov. Phys. Tech. Phys. **17**, 852 (1972)].
[5]V. S. Kozlov, M. V. Stabnikov, V. I. Tarakanov, and M. A. Tombak, Nucl. Instrum. Methods **140**, 125 (1977).
[6]M. Dykes, P. Lecoq, D. Gusewell *et al.*, Nucl. Instrum. Methods **179**, 487 (1981).
[7]F. R. Eisler, Nucl. Instrum. Methods **163**, 105 (1979).
[8]I. S. Klimenko, E. G. Matinyan, and I. P. Nalimov, Opt. Spektrosk. **26**, 1019 (1969).
[9]W. T. Welford, Appl. Opt. **5**, 872 (1966).
[10]A. I. Mel'nichenko and V. I. Silaev, Preprint ITÉF-9 [in Russian], ITEP, Moscow (1981).
[11]A. I. Mel'nichenko and V. I. Silaev, Preprint ITÉF-105 [in Russian], ITEP, Moscow (1981).
[12]J. L. Benichou, A. Herve, K. E. Johansson *et al.*, Nucl. Instrum. Methods **214**, 245 (1983).
[13]L. V. Bakanov, B. A. Vorob'ev, A. N. Zubarev *et al.*, Communication R13-84-285 [in Russian], JINR, Dubna (1984).
[14]L. V. Bakanov, V. D. Lebedev, and A. F. Naĭdenkov, Preprint 1163 [in Russian], LINP, Leningrad (1986).
[15]A. M. Bekker, N. I. Bukhtoyarova, and M. A. Tombak, Preprint 1014 [in Russian], LINP, Leningrad (1984).
[16]I. A. Mel'nichenko, Preprint ITÉF-12 [in Russian], ITEP, Moscow (1987).
[17]M. V. Stabnikov and M. A. Tombak, in: *Proceedings of the International Conference on Instrumentation for High Energy Physics* [in Russian] (Dubna, 1971), p. 382.
[18]V. I. Komarov and O. V. Savchenko, Nucl. Instrum. Methods **34**, 289 (1965).
[19]M. M. Kulyukin, M. V. Stabnikov, M. A. Tombak, and Yu. A. Shcherbakov, in: *Proceedings of the International Conference on Instrumentation for High Energy Physics*, edited by S. Stipeich (Frascati, Italy, 1973), p. 235.
[20]A. G. Kalimov, V. S. Kozlov, O. V. Lobanov *et al.*, Preprint LIYaF-407 [in Russian], LINP, Leningrad (1978).
[21]M. V. Stabnikov and M. A. Tombak, Preprint LIYaF-497 [in Russian], LINP, Leningrad (1979).
[22]M. A. Tombak, Preprint LIYaF-499 [in Russian], LINP, Leningrad (1979).
[23]A. G. Kalimov, V. S. Kozlov, M. V. Stabnikov *et al.*, Preprint LIYaF-518 [in Russian], LINP, Leningrad (1979).
[24]P. Ul'man, Kh. Ul'man, Yu. A. Shcherbakov, and K. Zeliger, Communication R13-12260 [in Russian], JINR, Dubna (1979).
[25]A. Budzyak, I. Ts. Ivanov, V. A. Panyushkin *et al.*, Preprint 1-80-299 [in Russian], JINR, Dubna (1980).
[26]A. Budzyak, I. Ts. Ivanov, V. S. Kozlov *et al.*, Communication 1-80-303 [in Russian], JINR, Dubna (1980).
[27]R. Rohrbach, J. J. Bonnet, and M. Cathenoz, Nucl. Instrum. Methods **111**, 485 (1973).
[28]L. Busso, M. M. Kulyukin, É. D. Lozanskiĭ *et al.*, Preprint R13-9131 [in Russian], JINR, Dubna (1975).
[29]I. V. Falomkin, M. M. Kulyukin, E. D. Lozansky *et al.*, Nucl. Instrum. Methods **131**, 431 (1975).
[30]L. Busso, M. M. Kulyukin, É. D. Lozanskii *et al.*, Zh. Eksp. Teor. Fiz. **70**, 785 (1976) [Sov. Phys. JETP **43**, 406 (1976)].
[31]A. G. Kalimov, V. S. Kozlov, M. V. Stabnikov *et al.*, Nucl. Instrum. Methods **185**, 81 (1981).
[32]P. Ul'man, Kh. Ul'man, Yu. A. Shcherbakov, and K. Zeliger, Preprint 13-81-321 [in Russian], JINR, Dubna (1981).
[33]É. Sodnomyn, Ban Khe Son, V. Ĭirka *et al.*, Communication R-13-87-312 [in Russian], JINR, Dubna (1987).
[34]I. V. Falomkin, I. Ts. Ivanov, N. N. Khovansky *et al.*, Nucl. Instrum. Methods Phys. Res. **A236**, 289 (1985).
[35]R. Majka, T. Cardello, S. Dhawan *et al.*, Nucl. Instrum. Methods **192**, 241 (1982).
[36]V. Eckardt and S. Wenig, Nucl. Instrum. Methods Phys. Res. **A234**, 606 (1985).
[37]L. Montanet and S. Reucroft, Phys. Rep. **83**, 61 (1982) [Russ. transl., Usp. Fiz. Nauk **142**, 635 (1984)].
[38]H. Drevermann, K. K. Geissler, and K. E. Johansson, Nucl. Instrum. Methods Phys. Res. **242**, 65 (1985).
[39]P. R. Hobson, D. C. Imrie, and G. J. Lush, Nucl. Instrum. Methods Phys. Res. **A239**, 155 (1985).
[40]H. Drevermann and W. Krischer, Nucl. Instrum. Methods Phys. Res. **A239**, 160 (1985).
[41]V. A. Goncharov, A. Yu. Zotov, É. P. Kistenev *et al.*, Preprint IHEP-86-107 [in Russian], IHEP, Serpukhov (1986).
[42]Yu. A. Belokopytov, A. P. Vorob'ev, V. A. Goncharov *et al.*, Preprint IHEP-86-106 [in Russian], IHEP, Serpukhov (1986).
[43]Yu. D. Aleshin, V. A. Goncharov, T. D. Karlov *et al.*, Preprint IHEP-4 [in Russian], IHEP, Moscow (1987).
[44]G. Stroke and R. Restrick, Appl. Phys. Lett. **7**, 229 (1965).
[45]A. W. Lohmann, J. Opt. Soc. Am. **55**, 1555 (1965).
[46]H. R. Worthington, J. Opt. Soc. Am. **56**, 1397 (1966).
[47]G. Cochran, J. Opt. Soc. Am. **56**, 1513 (1966).
[48]Yu. A. Bykovskiĭ, A. M. Zarubin, and A. I. Larkin, Zh. Tekh. Fiz. **55**, 2067 (1985) [Sov. Phys. Tech. Phys. **30**, 1216 (1985)].
[49]Yu. A. Bykovskiĭ, A. M. Zarubin, and A. I. Larkin, Kvant. Elektron. (Moscow) **13**, 1770 (1986) [Sov. J. Quantum Electron. **16**, 1165 (1986)].
[50]Yu. A. Bykovskiĭ, A. M. Zarubin, A. I. Larkin *et al.*, Communication R1-86-669 [in Russian], JINR, Dubna (1986).
[51]M. Born and E. Wolf, *Principles of Optics*, 4th ed. (Pergamon Press, Oxford, 1969) [Russ. transl., Nauka, Moscow, 1973].
[52]A.s. 1140085 SSSR, MKI[4] G 03 V 35/08, "A technique for stereoscopic photography" [in Russian], A. M. Zarubin and A. I. Larkin, Otkrytiya, Izobreteniya [Discoveries and Inventions], No. 6, 148 (1985).
[53]E. N. Linfoot and E. Wolf, Proc. Phys. Soc. (London) **B66**, 145 (1953).
[54]W. T. Welford, J. Opt. Soc. Am. **50**, 749 (1960).
[55]R. Bizzarri, Preprint CERN-EP-EHS-PH-81-11, CERN, Geneva (1981).
[56]R. Bizzarri and C. Schiller, Preprint CERN-EP-EHS-PH-81-13, CERN, Geneva (1981).
[57]L. M. Soroko, Communication D1-82-642 [in Russian], JINR, Dubna (1982).
[58]Gy. L. Bencze and L. M. Soroko, Preprint E13-84-310 [in English], JINR, Dubna (1984).
[59]J. H. McLeod, J. Opt. Soc. Am. **44**, 592 (1954).
[60]J. H. McLeod, J. Opt. Soc. Am. **50**, 166 (1960).
[61]J. Dyson, Proc. R. Soc. London Ser. A **248**, 93 (1958).
[62]I. A. Mikhaltsova, V. I. Nalivaiko, and I. S. Soldatenkov, Optik **67**, 267 (1984).
[63]V. M. Vedernikov, V. N. V'yukhin, V. P. Kir'yanov *et al.*, Avtometriya No. 3, 3 (1981).
[64]V. P. Koronkevich, V. P. Kirijanov, F. I. Kokoulin *et al.*, Optik **67**, 257 (1984).
[65]M. Rioux, R. Tremblay, and P. A. Belanger, Appl. Opt. **17**, 1532 (1978).
[66]O. Bryngdahl, J. Opt. Soc. Am. **61**, 169 (1971).
[67]O. Bryngdahl, J. Opt. Soc. Am. **60**, 915 (1970).
[68]M. A. Golub, S. V. Karneev, A. M. Prokhorov *et al.*, Pis'ma Zh. Tekh. Fiz. **7**, 618 (1981) [Sov. Tech. Phys. Lett. **7**, 264 (1981)].
[69]V. A. Danilov, V. V. Popov, A. M. Prokhorov *et al.*, Pis'ma Zh. Tekh. Fiz. **8**, 810 (1982) [Sov. Tech. Phys. Lett. **8**, 351 (1982)].
[70]A. V. Goncharskiĭ, V. A. Danilov, V. V. Popov *et al.*, Dokl. Akad. Nauk SSSR **273**, 605 (1983) [Sov. Phys. Dokl. **28**, 955 (1983)].
[71]A. V. Goncharskiĭ, I. N. Sisakyan, and V. V. Stepanov, Dokl. Akad. Nauk SSSR **279**, 68 (1984) [Sov. Phys. Dokl. **29**, 900 (1984)].
[72]A. V. Goncharskiĭ, V. A. Danilov, V. V. Popov *et al.*, Kvant. Elektron. (Moscow) **11**, 166 (1984) [Sov. J. Quantum Electron. **14**, 108 (1984)].
[73]A. V. Goncharskiĭ, V. A. Danilov, V. V. Popov *et al.*, Kvant. Elektron. (Moscow) **13**, 660 (1986) [Sov. J. Quantum Electron. **16**, 432 (1986)].
[74]V. S. Akopyan, Yu. K. Danilenko, V. A. Danilov *et al.*, Kvant. Elektron. (Moscow) **12**, 401 (1985) [Sov. J. Quantum Electron. **15**, 262 (1985)].
[75]L. M. Soroko, "Mesooptics, holography, and the optical processor," in: *Techniques and Instrumentation for Optical Holography* [in Russian] (Leningrad Nuclear Physics Institute, Leningrad, 1983), p. 189.
[76]A. Faggiano, C. Gadda, P. Moro *et al.*, Proc. Soc. Photo-Opt. Instrum. Eng. **656**, 213 (1986).
[77]A.s. 743424 SSSR, MKI[2] G 01 T 5/10, G 03 H 5/00, "A device for automatically measuring the angular distributions of particle tracks" [in Russian], L. M. Soroko, Otkrytiya, Izobreteniya [Discoveries and Inventions], No. 21, 262 (1981).
[78]A. Ya. Astakhov, G. M. Komov, V. I. Sidorova *et al.*, Communication R13-83-119 [in Russian], JINR, Dubna (1983).
[79]Gy. Bencze and L. M. Soroko, Communication R13-85-136 [in Russian], JINR, Dubna (1985).
[80]Gy. Bencze and L. M. Soroko, Communication R13-85-137 [in Russian], JINR, Dubna (1985).
[81]Gy. Bencze and L. M. Soroko, Communication R13-85-138 [in Russian], JINR, Dubna (1985).
[82]A. Ya. Astakhov, Gy. Bencze, Ya. Beg *et al.*, Communication R13-87-275 [in Russian], JINR, Dubna (1987).
[83]Gy. L. Bencze and L. M. Soroko, Communication E13-87-387 [in English], JINR, Dubna (1987).
[84]Gy. L. Bencze and L. M. Soroko, Communication E13-87-389 [in English], JINR, Dubna (1987).
[85]Gy. L. Bencze and L. M. Soroko, Communication E13-87-388 [in English], JINR, Dubna (1987).
[86]Gy. Bencze, A. Kishvaradi, G. Nitran, and L. M. Soroko, Comunica-

tion R13-86-630 [in Russian], JINR, Dubna (1986).
[87]A.s. 124960 SSSR, MKI[4] G 01 T 5/02, "A setup for scanning nuclear photoemulsion" [in Russian], L. M. Soroko, Otkrytiya, Izobreteniya [Discoveries and Inventions], No. 29, 233 (1986).
[88]Gy. Bencze and L. M. Soroko, Communication R13-86-659 [in Russian], JINR, Dubna (1986).
[89]Gy. Bencze, I. G. Pal'nikova, A. G. Poleshchuk, and L. M. Soroko, Communication R13-86-240 [in Russian], JINR, Dubna (1986).
[90]P. Koronkevich, G. A. Leĭkova, I. G. Mikhal'tsova *et al.*, Avtometriya No. 1, 4 (1985).
[91]V. P. Koronkevich, I. G. Pal'chikova, A. G. Poleshchuk, and Yu. I. Yurlov, Preprint No. 265 [in Russian], Institute of Automation and Electrometry, Novosibirsk (1985).
[92]L. M. Soroko, Preprint E13-87-292 [in English], JINR, Dubna (1987).
[93]L. M. Soroko, *Hilbert Optics* [in Russian] (Nauka, Moscow, 1981).
[94]J. W. Ogland, Appl. Opt. **17**, 2917 (1978).
[95]Gy. Bencze and L. M. Soroko, Communication R13-87-594 [in Russian], JINR, Dubna (1987).
[96]L. M. Soroko, Communication R13-87-527 [in Russian], JINR, Dubna (1987).
[97]L. M. Soroko, Communication R13-87-169 [in Russian], JINR, Dubna (1987).
[98]L. M. Soroko, Communication R13-87-170 [in Russian], JINR, Dubna (1987).
[99]L. M. Soroko, Communication R13-87-358 [in Russian], JINR, Dubna (1987).
[100]Gy. Bencze and L. M. Soroko, Communication R13-85-502 [in Russian], JINR, Dubna (1985).
[101]Gy. Bencze, I. G. Pal'chikova, A. G. Poleshchuk, and L. M. Soroko, Communication R13-87-174 [in Russian], JINR, Dubna (1987).
[102]A.s. 1121637 SSSR, MKI[3] G 01 T 5/10, "A device for multichannel scanning of nuclear photoemulsion" [in Russian], L. M. Soroko, Otkrytiya, Izobreteniya [Discoveries and Inventions], No. 40, 138 (1986).
[103]A. Ya. Astakhov, Gy. Bencze, A. Kishvaradi *et al.*, Communication R13-85-378 [in Russian], JINR, Dubna (1985).
[104]L. M. Soroko, Communication R13-87-468 [in Russian], JINR, Dubna (1987).
[105]A.s. 1234796 SSSR, MKI[4] G 01 T 5/10, "A device for observing particle tracks in nuclear photoemulsion [in Russian], L. M. Soroko, Otkrytiya, Izobreteniya [Discoveries and Inventions], No. 20, 203 (1986).
[106]C. J. R. Sheppard and A. Choudhury, Opt. Acta **24**, 1051 (1977).
[107]T. Wilson, Appl. Opt. **20**, 3238 (1981).
[108]C. J. R. Sheppard, D. K. Hamilton, and I. J. Cox, Proc. R. Soc. London, Ser. A **387**, 171 (1983).
[109]T. Wilson and C. J. R. Sheppard, *Theory and Practice of the Scanning Optical Microscope* (Academic Press, London, 1984).
[110]A.s. 1183934 SSSR, MKI[4] G 02 V 21/00, "A microscope" [in Russian], L. M. Soroko, Otkrytiya, Izobreteniya [Discoveries and Inventions], No. 37, 191 (1985).
[111]L. M. Soroko, Communication R13-87-576 [in Russian], JINR, Dubna (1987).
[112]A.s. 1273861 SSSR, MKI[4] 2 V 21/00, "A microscope" [in Russian], L. M. Soroko, Otkrytiya, Izobreteniya [Discoveries and Inventions], No. 44, 180 (1986).
[113]L. M. Soroko, *Introscopy* [in Russian] (Énergoatomizdat, Moscow, 1983).

Translated by Patricia Millard